Time-scales of a Dune-Beach System and Implications for Shoreline Modelling

Jennifer Montaño[1], Giovanni Coco[1], Teddy Chataigner[2], Marissa Yates[2], Nicolas Le Dantec[3], Serge Suanez[4], Laura Cagigal[1], France Floc'h[4], Ian Townend[5]

[1] School of Environment, Faculty of Science, University of Auckland, Auckland, 1142, New Zealand.

2 Saint-Venant Hydraulics Laboratory & ENPC.

3 Laboratoire Géosciences Océan & Cerema

4 Université de Bretagne Occidentale

5 University of Southampton

Corresponding author: Jennifer Montano (jmon177@aucklanduni.ac.nz)

Key Points:

- A centroid analysis and shoreline modelling identified the influence of the dune system on shoreline evolution over a range of time-scales.
- Different beach migration modes (steepening/flattening and advance/retreat) were identified using a centroid analysis
- Our analysis showed that time-scales related to dune erosion and recovery play an important role in shoreline modelling performance.

Abstract

Understanding the interactions between dune systems and beaches is critical to determining the short-term shoreline response and the long-term resilience. In this study, almost 15 years of monthly beach/dune measurements were analysed for three different profiles at Vougot Beach, France to understand and predict shoreline changes from intra- to multi-annual time- scales. Four migration modes: advance/retreat (translation modes) and steepening/flattening (rotation modes) were identified through a centroid analysis. The analysis showed that translation and rotation can occur simultaneously, with long-term trends of beach retreat and profile steepening (lower beach retreating and upper beach advancing), which was interrupted by two energetic wave events causing profile flattening (lower beach advancing and upper beach retreating). These two observations are evidence of how the sediment contribution resulting from the dune erosion events temporarily caused a large advance in the shoreline position. A recent modelling approach that accounts for different time-scales is applied to predict the shoreline changes, showing significant improvements in comparison to a traditional shoreline equilibrium model when time-scales related with the dune erosion and recovery are considered. The results showed that the dune system affects the beach profile evolution both spatially, with different impacts at different elevations along the cross-shore profile, and temporally, by periodically redistributing the sediment in the system.

1 Introduction

Over the last few years, research efforts to understand and predict shoreline evolution have increased because of the increased threat posed by climatic changes, including changes in

sea levels as well as changes in storm magnitude and frequency. Sediment exchange across the beach occurs over different time-scales, and many uncertainties in the beach/dune response to different drivers still exists on scales ranging from storms to the overall wave climate. The processes involved are further complicated by the stochastic nature of the forcing and the inherent non-linear interactions and feedbacks operating over multiple temporal and spatial scales (Hapke et al., 2016; Larson & Kraus, 1995).

It is becoming increasingly clear that, due to climatic changes, coastal erosion is likely to be exacerbated. Sea Level Rise (SLR) has been the focus of the attention of the beach community in the last couple of decades (Le Cozannet et al., 2019; Nicholls & Cazenave, 2010), but it is becoming evident that shoreline erosion is not only affected by SLR but also by changes in the (storm) wave climate (Masselink et al., 2016). For example, Barnard et al. (2015) found that El Niño and La Niña events in the Pacific Ocean basin might lead to extreme coastal erosion and flooding, independent of sea level rise. The importance of storms was also reported along the Atlantic Coast of Europe during the 2013/2014 winter, which was the most energetic winter since 1948 (Masselink et al., 2016; Matthews et al., 2014) causing unprecedented dune and beach erosion on Northern European Atlantic beaches (Blaise et al., 2015; Burvingt et al., 2018; Castelle et al., 2015; Dissanayake et al., 2015; Masselink et al., 2016; Pérez-Alberti & Trenhaile, 2015). Therefore, models that can accurately predict shoreline changes over both short (storm) and mid horizons (wave climate) are required. D'Anna et al. (2020) studied the uncertainty associated with different variables using a cross-shore-only version of the LX-Shore shoreline change model (Robinet et al., 2018) where SLR effects are included using the Bruun Rule. When applied to reproduce 20 years of shoreline evolution at Truc Vert beach, France, they found that the free parameters (response rate, linear trend, and beach memory) used to model intra to multi-

annual time-scales resulted in larger contributions to the overall uncertainty than the SLR or depth of closure (used in applying the Bruun Rule). This highlighted a major problem in long-term predictions, since climate change may significantly impact the wave climate and the extremes, complicating the use of model parameters calibrated using past data (D'Anna et al., 2020).

During storms, the shoreline typically moves landward (erosion), while during calm periods the shoreline typically moves seaward (accretion). Shoreline changes occurring over much larger time-scales (decadal to centennial) may be the result of other factors such as longshore sediment transport, changes in sediment supply, anthropogenic interventions, sea level rise (SLR), and changes in the wave climate, amongst others (Bruun, 1988; Hanson, 1989; Vitousek et al., 2017a). Generally, cross-shore sediment transport is considered to be the main control of shoreline evolution at seasonal and inter-annual time-scales (Kriebel & Dean, 1985; Miller & Dean, 2004), whilst longshore processes (specifically on open coastlines) become dominant over much longer time-scales (decadal to centennial) (Ashton et al., 2001; Hanson, 1989; Hurst et al., 2015). Nonetheless, factors such as chronological order of storms (Callaghan et al., 2008; Coco et al., 2014; Senechal et al., 2015), phase of the tide (Castelle et al., 2014; Lemos et al., 2018), and variable water levels (Ruggiero et al., 2001; Serafin & Ruggiero, 2014) may also have an important role in interpreting dune/beach coupled dynamics. In addition, the antecedent morphological conditions, such as, shoreline orientation and exposure to incoming waves, bar morphology among others, may also have significant impacts on the shoreline

response (Blossier et al., 2017; Castelle et al., 2010; Davidson et al., 2013; Miller & Dean, 2004; Yates et al., 2009).

Uncertainties in the prediction of dune/beach system changes are still large due to limited knowledge of the interactions between the physical drivers and the system response, which occur over a range of time-scales. For instance, short-term dune/beach erosion during storms may cause abrupt changes to the coastal system with long-lasting effects. Drivers that control dune/beach erosion and subsequent recovery are likely to be different, and therefore the time-scales associated with such processes will also be different. For example, erosion is usually fast and episodic (hours to days), while recovery is often slow and long-term (months to years), and the physical processes and therefore time-scales are different for dunes and beaches (Burvingt et al., 2018; Dodet et al., 2019). Recently, Conlin et al.(2020) used a hybrid Surface Empirical Orthogonal Functions to show that storm impacts can generate persistent topographic features that remain visible for months to years, generating a feedback that influences the response to future storms along different portions of the elevation profile as well as the alongshore variability. This can overwhelm the seasonal topographic signal associated with seasonality in water levels and storminess.

Dune erosion has been found to be a result of wave and water level action mobilising and removing sediment from the dune/berm and depositing it offshore. Nonetheless, Cohn et al., (2018) found that high water levels, along with wind-induced sediment transport, may also contribute to dune growth. Erosion along the upper beach has been attributed mainly to interactions between the impacts of incident waves and the antecedent morphology of the sub-aerial and subaqueous beach (Coco et al., 2014; Splinter et al., 2014). In addition, dune recovery

by wind-blown sand occurs over significantly longer time scales compared to the recovery of the upper beach (Morton et al., 1994; Phillips et al., 2019).

Although the external drivers that control dune and beach erosion and subsequent recovery may vary, feedbacks between both parts of the dune/beach system play an important role. For dunes to recover, a sediment supply source is needed. This requires first that the beach recovers, through the onshore migration and welding of nearshore bars, which is in turn followed by accretion along the backshore to generate a sediment source for dune recovery (Houser, 2009; Larson et al., 2016). On the other hand, dune erosion is controlled not only by the duration of time that wave run-up reaches the dune toe, but also by the width of the beach immediately fronting the dune, since the berm reduces the wave energy reaching the dune (Beuzen et al., 2019; Houser, 2009; Plant & Stockdon, 2012).

In recent decades, data availability has increased, with long time-series from camera systems (Montaño et al., 2020; Phillips et al., 2017), LiDAR measurements (Phillips et al., 2019), advances in satellite remote-sensing (Luijendijk et al., 2018; Vos et al., 2019), or longer time span topo-bathymetric measurements (Ludka et al., 2019; Turner et al., 2016) encouraging the development of shoreline change models using data-driven approaches. For instance, equilibrium models (Davidson et al., 2013; Yates et al., 2009), also called Hybrid models (Montaño et al., 2020a), have become popular due to their simplicity, low computational cost and good performance in predicting shoreline changes at intra-annual to multi-annual time-scales. This type of model is based on the dis-equilibrium concept (Wright et al., 1985), in which the shoreline position rate of change is governed by the difference between present and equilibrium wave and/or morphological conditions (Davidson et al., 2013; Miller & Dean, 2004; Yates et al., 2009). This type of model relies heavily on data to search for and optimize the

model free parameters (Splinter et al., 2013). As one might expect, the performance of these cross-shore models is poor at locations where the driver of shoreline changes is long-shore sediment transport (Dodet et al., 2019). To fill this gap, Vitousek et al., (2017b) added a new term to the cross-shore model based on Yates et al. (2009). The new term accounts for longshore processes through a 'one-line' model approach (US Army Corps of Engineers, 1984). The authors also added a term that accounts for SLR-induced shoreline recession based on the 'Bruun rule' (Bruun, 1962), in addition to a long-term trend term taking into account unresolved processes. Robinet et al. (2018) followed a similar approach and proposed a model integrating the cross-shore component based on the ShoreFor model of Davidson et al. (2013), which also includes a long-term trend term, and an alongshore component similar to Ashton et al. (2001). A more recent improvement to the this type of model was introduced by Antolínez et al. (2019), which included the contribution of foredune erosion, in addition to the cross- and long-shore changes. Despite the level of complexity of the model, the berm profile was fixed, and dune recovery was neglected. Other types of more complex process-based models calculating 2D or 3D sediment transport processes have been proposed to simulate dune/beach changes from intra- to multi-annual temporal scales (Hanson et al., 2010; Larson et al., 2016; Palalane et al., 2016). However, their applicability remains to be tested, and in some cases, process-based models have not shown better performance than simpler equilibrium-based hybrid models (Splinter & Palmsten, 2012).

Hapke et al. (2016) found that shoreline change patterns representing responses to different oceanographic forcing factors can often be separated, and shoreline response can be resolved on time-scales ranging from storm events to decadal variations. Montaño et al. (2021) presented a different approach to equilibrium models in which shoreline changes are predicted by

isolating and associating time-scales in the drivers and the shoreline response. The method hypothesizes that shoreline changes at a specific time-scale can be predicted using the drivers at the same temporal scale. For instance, seasonal shoreline changes might be predicted using only seasonal oscillations in the drivers while the total shoreline change results from the summation of different time-scales (e.g., seasonal, annual, bi-annual, decadal). As in equilibrium models, this approach heavily relies on data to identify the important time-scales and to calculate the free coefficients that link drivers and shoreline response at different time-scales. This model approach also uses the Sea Level Pressure (SLP) fields and gradients to predict the shore- line changes, since SLP might contain information not present in the bulk waves parameters ($\boldsymbol{H_s, T_p, \theta}$), such as, mean water level fluctuations, wave generation areas and information of large atmospheric anomalies.

Models of shoreline evolution often struggle to link observed changes to the incident wave field. We hypothesize that because of the many timescales involved, shoreline evolution models fail to capture the dynamic form of the beach (which reflect stored mass, or enhanced dissipation) and, in particular, the role of dune-beach interactions in the profile response to specific events. The aim of the present study is to analyse dune-beach behaviour in the context of shoreline modelling, using almost 15 years of observations of monthly subaerial beach/dune profiles collected in a macro-tidal beach, Vougot, France (Suanez et al., 2016) (Section 2.1). To do so, the SPADS (Shoreline Prediction At Different time-Scales) model (Montaño et al., 2020) is used to analyse the dominant time-scales of observed changes at different elevations along the intertidal profile and predict shoreline changes (Section 2.2). The beach migration modes (steepening, flattening, advance and retreat) were identified through a profile centroid analysis (Section 2.3). Results of both the analysis and the shoreline predictions using SPADS are

175 presented and discussed the section 3 and 4, where the influence of dune events on shoreline
176 changes and the implications for the shoreline modelling are also discussed. Finally, the key
177 findings and conclusions are summarized in section 5.

178 **2 Methods**

179 2.1 Study area

180 Vougot is a 2 km long beach located on the north coast of Finistère in Brittany (France) in the
181 municipality of Guissèny (Figure 1a). The beach is characterized by a macro-tidal range,
182 reaching 8.5 m (referring to astronomic tide), which can expose more than 400 m of the intertidal
183 profile at low tide. The beach is backed by an extensive dune system that varies from 200 m to
184 400 m wide, with a dune sediment size $D_{50} \sim 0.20$ mm, which becomes coarser on the beach
185 ($D_{50} \sim 0.25$ - 0.315 mm). The beach is fronted by a rocky shore platform with the presence of
186 islets and reefs that shelter the coast, giving the dune system a convex curved shape (Suanez et
187 al., 2012).

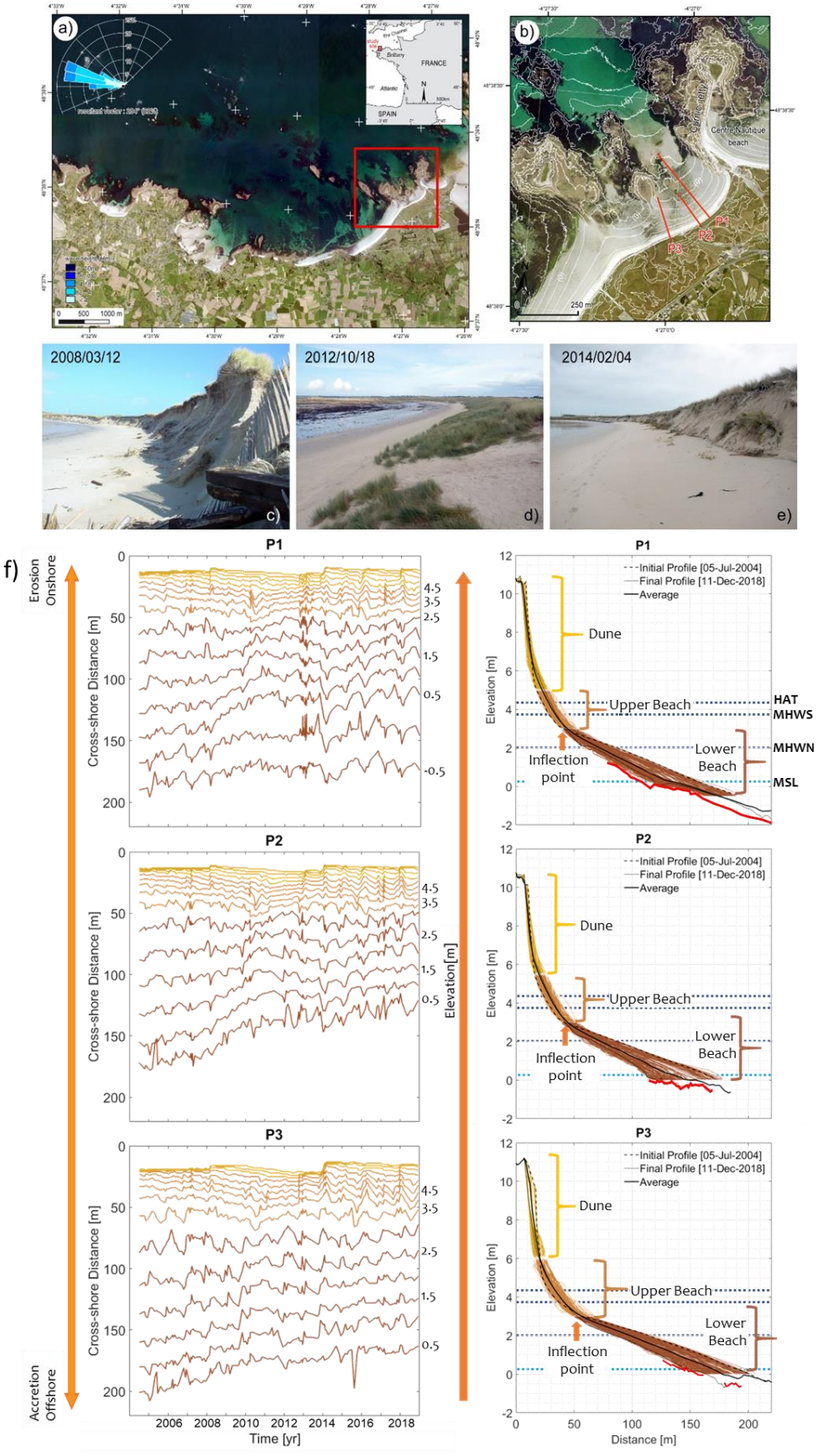
a)
b)
FRANCE
SPAIN
Brittany
Atlantic
Centre Nautique beach
P1
P2
P3
250 m
2008/03/12
2012/10/18
2014/02/04
c)
d)
e)
f)
Erosion
Onshore
Accretion
Offshore
Cross-shore Distance [m]
Elevation [m]
Time [yr]
2006 2008 2010 2012 2014 2016 2018
4.5
3.5
2.5
1.5
0.5
-0.5
Initial Profile [05-Jul-2004]
Final Profile [11-Dec-2018]
Average
Dune
Upper Beach
Lower Beach
Inflection point
HAT
MHWS
MHWN
MSL
Distance [m]

Figure 1. Study site. a) Location of Vougot beach, France, with the location of the modelled waves (wave rose; blue dot); b) Dune erosion event: 2008/03/12; c) Dune recovery: 2012/10/18; d) Detail of Vougot beach identifying the three profiles (red lines) analysed in this study; e) Dune erosion event: 2014/02/04. f) Contour elevation position time series (left panels) for elevations ranging from lower intertidal zone to over upper intertidal zone and dune. Beach profile evolution during the study period (2004 to 2018) along the intertidal zone (right panels) for Profile 1 (P1), Profile 2 (P2), and Profile 3 (P3). Red lines represent the hard bottom (clay and/or rocky and/or peat outcrops). Dashed dark blue lines represent the Highest Astronomic Tide (HAT), Mean High Spring (MHWS) and Mean High Water Neap (MHWN) respectively. Dashed light blue lines represent the Mean Sea Level (MSL). Images a and b Institut National de l'Information Géographique.

Monthly sand level observations of the sub-aerial beach/dune profile (Figure 1f) from nearly 15 years (2004/07/05 to 2018/12/11) were collected using a DGPS Trimble 5800/5700 and a Topcon HYPER-II, in RTK mode with errors reaching up to ± 5 cm in x, y, and ± 2 cm in z. Data were analyzed for three profiles located in the eastern part of the beach, near the jetty of Curnic, which connects the Enez Croaz-Hent islet to the coast (Figure 1b, red lines). Although the shoreline is generally defined as the physical interface between land and water (Boak & Turner, 2005), on macro-tidal beaches where the cross-shore length is of the order of hundreds of meters, an exact shoreline definition is difficult to obtain (Castelle et al., 2014). In this study, different elevations are used as a proxy for the shoreline cross-shore position ($\boldsymbol{S = f(z)}$) where z

represents the different elevations. Temporal changes in contour elevations ('shoreline') each 0.5 m are displayed in Figure 1f, left panels.

In recent decades, the dune system experienced significant retreat, especially along the eastern part of Vougot beach, with most of the material transported to the west, contributing to building-up the western section of the beach (Suanez et al., 2010, 2012). This erosion has been attributed to the construction of the jetty of Curnic in 1974, which modified the local hydrodynamics, interrupting the westward sand drift and inducing a scarcity of sediment over the eastern, downdrift part of the Vougot beach/dune system. In addition, the beach is characterized by a rocky platform in the tidal zone, with relief in the form of small islets and reefs that cause wave diffraction and complex current patterns, especially impacting longshore currents (Suanez et al., 2010, 2012). Along the three analysed profiles, the presence of different types of "hard bottom" (red lines, Figure 1f, right panels), e.g., periglacial deposits (clay), rocky or peat outcrops, or Pleistocene/Holocene gravel accumulation, limits sand availability. During some periods of the year, these hard surfaces are no longer covered by sand, especially along the lower part of the profiles.

Suanez et al. (2012) carried out a detailed analysis of the dune recovery after the storm 'Johanna' hit the French Atlantic coast in March 10, 2008, which caused severe dune erosion (Figure 1c) (Suanez & Cariolet, 2010). The subsequent phase of dune recovery, which lasted from 2008 to 2013 (Figure 1d) was characterized by growth of vegetation and the construction of 'secondary' embryo dunes, reduced the impact of the storm surge. Another severe dune erosion event occurred during the 2013/2014 winter (Figure 1e), considered one of the most energetic winters along the Atlantic coast of Europe since 1948 (Masselink et al., 2016a). Three energetic winter storms (January, February, and March) coincided with large spring high tides, augmenting

the effects of the storm surge, with important implications for the dune-beach system (Blaise et al., 2015; Masselink et al., 2016; Suanez et al., 2016). The current study evaluates both dune erosion events and the subsequent recovery phases.

2.2 The SPADS Model

Montaño et al. (2021) introduced and tested a new model for Shoreline Prediction At Different time-Scales (SPADS) based on identifying the time-scales of drivers and shoreline change using the Complete Ensemble Empirical Mode Decomposition (CEEMD) method (Huang et al., 1998; Torres et al., 2011), and then linking the resulting time-scales with calibrated parameters. The model showed good performance compared with a traditional equilibrium model when tested at two cross-shore dominated beaches (Narrabeen, Australia and Tairua, New Zealand). CEEMD is a noise-assisted data analysis approach based on the Empirical Mode Decomposition (EMD) introduced by Huang et al. (1998). EMD-based methods were designed to identify non-linear and non-stationary oscillations in data, assuming that simple oscillatory modes of significantly different superimposed frequencies coexist (Huang et al., 1998). EMD decomposes time series into a finite set of 'intrinsic mode functions' (IMFs), representing different time-scales with varying amplitudes and frequencies (the last IMF is considered to be the trend). CEEMD improves on EMD, by assisting the IMF separation through the addition of Gaussian white noise to the signal and the true IMF is calculated as the mean of an ensemble (100 realizations in our study).

Modelling with SPADS consists of a number of steps, starting with the decomposition of the time-series of shoreline and drivers using the CEEMD method. Then, a statistical test (Wu & Huang, 2004) is applied to identify the significant IMFs obtained using the CEEMD approach (only the IMFs that satisfied a significance level higher than 95% were selected for further

analysis). The reconstruction of the shoreline changes at each individual time-scale is performed through an optimization analysis to find the coefficients that link driver and shoreline changes by maximizing the Mielke's modification index λ (Duveiller et al., 2016). The total shoreline position is reconstructed as the summation of the different time-scales. The CEEMD method needs to be run multiple times with different white noise initializations (we used white noise amplitudes between 0.1 and 0.5 of the signal standard deviation). The final shoreline position is the average of the shoreline positions obtained with the different levels of white noise. The SPADS model uses two type of drivers: large-scale two-dimensional SLP fields and gradients from Climate Forecast System Reanalysis (CFSR), and wave bulk parameters. The first step to obtain the SLP information is to find the influence area with the ESTELA (Evaluating the Source and Travel time of the wave Energy reaching a Local Area) method (Pérez et al., 2014). This method evaluates the source and travel time of waves reaching a given location based on the geographic criteria and the two-dimensional wave spectra (see Rascle & Ardhuin, 2013). In order to account for the travel time of swell waves in the analysis, the SLP information is modified according to the isochrones of the average travel time as in Hegermiller et al. (2017) (Figure 2a). After the SLP field and gradients is modified with the ESTELA method, a Principal Component Analysis (PCA), a statistical technique widely used in climatology to identify dominant variability patterns and reduce dimensionality (Camus et al., 2014; Rueda et al., 2019), is performed.

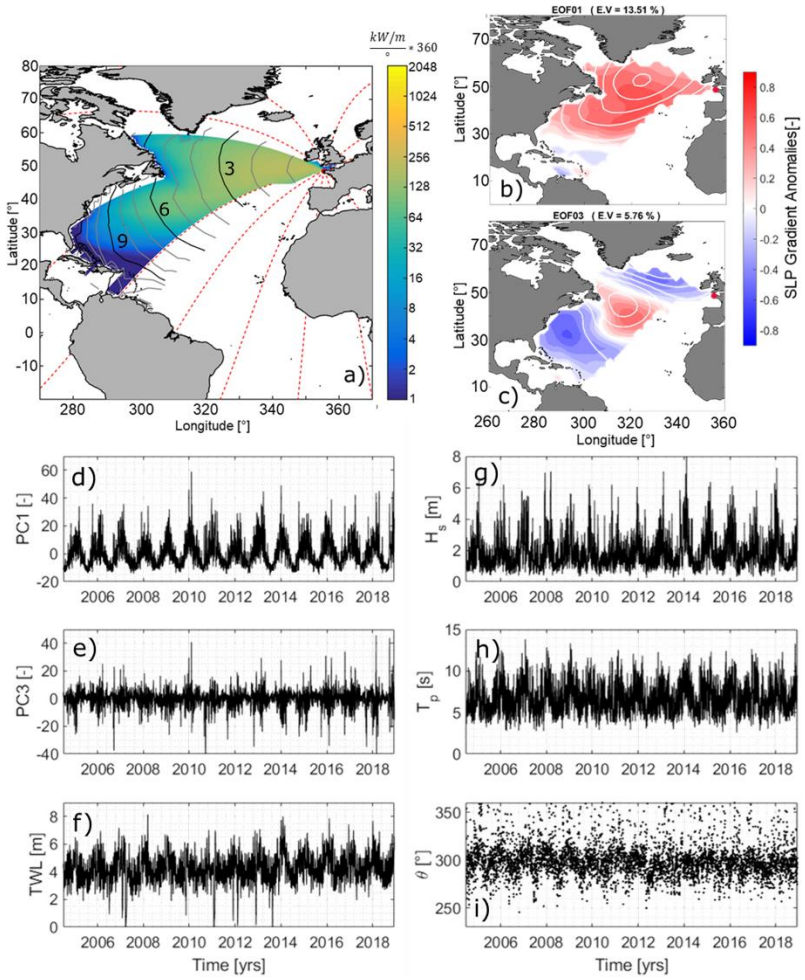

Figure 2. Model Drivers. a) mean energy flux for all possible source points (calculated using ESTELA). The travel time (in days) is represented by the black lines (3-day increments) and grey lines (1 day increments). Red dotted lines represent the great circles; b) and c) examples of the first and third Empirical Orthogonal Functions (EOFs) of the SLP fields and gradients. Shaded areas represent SLP gradients, while the contours represent SLP fields; d) and e) examples of the corresponding Principal Components (PCs) for b) and c) used as drivers for the

CEEMD model; f) total water levels (TWL) and g) to i) bulk wave bulk parameters used for the analysis ($\boldsymbol{H_s, T_p, \theta}$).

The PCA projects the original data on a new space, searching for the maximum variance of the sample data. The dominant spatial variability patterns, called Empirical Orthogonal Functions or EOFs (Figure 2b and c), and temporal coefficients, i.e., Principal Components or PCs (Figure 2d and e), are used to reconstruct the original predictor X(x, t) with a linear combination of EOFs and PCs, where N is the is the number of selected EOFs:

$$\boldsymbol{X(x,t_i) = EOF_1(x)PC_1(t_i) + EOF_2(x)PC_2(t_i) + \cdots + EOF_N(x)PC_N(t_i)} \quad (\mathbf{1})$$

Following Montaño et al. (2021) we only used the first ten PCs (i.e., $\boldsymbol{N}$=10), which explain up to 54% of the overall variance. As discussed in Montaño et al. (2021), this analysis including the use of SLP and its gradients allows tracking wave information from a large generation area, avoiding reducing the large-scale variability to a single bulk wave parameter, which would ignore the complexities of the wave spectra. For example, it would ignore wave bi-modality which has been found important in different coastal processes, such as run-up and beach rotation (Montaño et al., 2020b; Wiggins et al., 2020). On the other hand, the wave information considers bathymetric effects that are not captured by SLP. Thus, in this study both drivers are used to predict shoreline changes. As discussed in Montaño et al. (2021), the model allows including any driver relevant for shoreline prediction (e.g., waves, winds, water levels) at both local and regional scales. More information about the model development can be found in Montaño et al. (2021).

Wave parameters in 43 m water depth (Figure 1a) were obtained using the numerical model WaveWatch3 run by the Ifremer (Boudière et al., 2013) (Figure 2g-h). As can be seen in

Figure 1a, waves arrive principally from the northwest (2004 to 2019). The beach is partially sheltered from the direct impact of Atlantic swell, and relatively well protected from waves originating in the west to northwest by an offshore platform scattered with islets and reefs that emerge at low tide (Masselink et al., 2016; Suanez et al., 2012). Since dune erosion events are important at Vougot, the Total Water Level (TWL) is also included in the analysis, with tide measurements from the Roscoff tide gauge station located about 30 km to the east of the survey area (Suanez et al., 2012). The maximum wave run-up ($\boldsymbol{R_{max}}$) was computed using an existing formula provided by (Cariolet & Suanez, 2013; Suanez et al., 2015), which has been calibrated using field measurements for Vougot Beach as, $\boldsymbol{R_{max} = 0.68 H_0 \xi_0}$, with $\boldsymbol{\xi_0 = \frac{tan\beta}{\sqrt{H_0/L_0}}}$, where $\boldsymbol{H_0}$ and $\boldsymbol{L_0}$ are the offshore wave height and wave length, and the beach slope $\boldsymbol{\beta}$ corresponds to the active section of the upper part of the beach, which in macro-tidal environments was found to estimate more accurately run-up predictions (Suanez & Cariolet, 2013).

To analyse the influence of the different time-scales on shoreline prediction, we compared the SPADS model with the ShoreFor model (Davidson et al., 2013). ShoreFor is one of the most widely applied shoreline models due to its simplicity and high performance (Dodet et al., 2019; Montaño., 2020a; Splinter et al., 2014). The model is based on the equilibrium concept so that cross-shore changes in the shoreline position are proportional to the incident wave power and the degree of disequilibrium. For wave conditions more energetic than equilibrium the beach is eroded and vice-versa. The model has two free parameters: a disequilibrium term which depends of the 'memory decay' of the beach (related with the dominant time-scale) and a linear trend term which accounts for additional processes not directly included in the model

formulation (e.g., longshore sediment transport). Detailed information about the ShoreFor model can be found in Davidson et al. (2013)

2.3 Centroid Analysis of beach profile changes

of adjustment can be identified for any beach profile: flattening and steepening (cross-shore beach profile rotation around a pivot point, Figure 3 quadrants I and III), and advancing and retreating (cross-shore beach profile translation, Figure 3, quadrants II and IV). These principal modes can also be combined to give more complex modes of rotation and translation, as observed on many coasts (Soulsby et al., 1999; Townend et al., 1990).

In the rotation modes, the cross-shore profile does not retreat or advance as an equilibrium profile but evolves towards a flatter or steeper profile around a pivot point (nodal point). The flattening mode consists in upper beach erosion and lower beach accretion causing a decrease in the beach slope, while the steepening mode displays the opposite behaviour (upper beach accretion and lower beach erosion, causing an increase in the beach slope). In the translation modes, the beach profile response is vertically uniform, and no pivot point is observed (see the schematic in Figure 3a). In addition, steepening/flattening can occur with no net change in profile volume, whereas retreat/advance implies a change in volume within the control volume. Although migration modes generally have been computed using beach volumes (e.g., Burvingt et al. 2017), a volumetric centroid analysis was used here to estimate beach migration modes following Taylor (2004) and Villamarin, (2017).

The centroids, here defined as a measure of the volumetric centre of the profile, were computed using the CoastalTools package (Townend, 2018). Cross-shore variations of the centroid (X horizontal axis) and vertical centroid variations (Z vertical axis) are computed from the first

moments calculated using the cross sectional control area defined by a rectangle (Figure 3b). Inside the control area, the following parameters are calculated:

Volume: $$\boldsymbol{V = \int z' dx'} \quad (\mathbf{2})$$

Horizontal centroid: $$\boldsymbol{X = \int x' z' dx' / V} \quad (\mathbf{3})$$

Vertical centroid $$\boldsymbol{Z = \int x' z' dz' / V} \quad (4)$$

where $\boldsymbol{x'}$ and $\boldsymbol{z'}$ are the horizontal and vertical distance from the origin ($\boldsymbol{x_{min}}$, $\boldsymbol{z_{min}}$) of the control area (Figure 3b):

$$\boldsymbol{x' = x - x_{min};\ x' \geq 0} \text{ and } \boldsymbol{z' = z - z_{min};\ z' \geq 0} \quad (5)$$

The total beach and dune volumes were computed using the defined control area ($\boldsymbol{V_T}$, black dashed square and $\boldsymbol{V_D}$, red dashed square, Figure 3b). These areas were based on the lower limits of the survey data, with $\boldsymbol{x_{T,min} = 0}$ m for the three profiles, and with $\boldsymbol{z_{T,min} = 0.5}$ m for Profile 1 and $\boldsymbol{z_{T,min} = 0}$ m for Profiles 2 and 3. The intertidal volumes considered here are likely to be less than the total sediment volume out to the closure depth and may not represent the total nearshore sediment volume. For the dune control area, we assumed that the dune toe elevation remained fixed based on the field observation for the initial measurement (red dot, Figure 3b). Then, $\boldsymbol{x_{D,min} = 0}$ m for the computation of the dune volumes at the three profiles, while $\boldsymbol{z_{D,min} = 5}$ m,

($\boldsymbol{x}$ = 18 m) for Profiles 1 and 2, and $\boldsymbol{z_{D,min} = 5.6}$ m, ($\boldsymbol{x}$ = 21 m) for Profile 3 based on the dune toe location in the initial measurements.

With the aim of comparing directly different profiles, the non-dimensional centroid coordinates $\boldsymbol{x_1}$, $\boldsymbol{z_1}$ are computed as:

Non-dimensional volume: $$\boldsymbol{m_0 = \int z'' dx''} \quad (6)$$

Non-dimensional horizontal centroid: $$\boldsymbol{x_1 = \int x'' z'' dx'' / m_0} \quad (7)$$

Non-dimensional vertical centroid $$\boldsymbol{z_1 = \int x'' z'' dz'' / m_0} \quad (8)$$

where $\boldsymbol{x''}$ and $\boldsymbol{z''}$ are defined as:

$$\boldsymbol{x'' = \frac{x'}{L_x}} \text{ and } \boldsymbol{z'' = \frac{z'}{L_z}} \quad (9)$$

with $\boldsymbol{L_x = \max(x')}$ and $\boldsymbol{L_z = \max(z')}$

3 Results

3.1 Dune influence on shoreline behaviour

Through the non-dimensional centroid maps, three "clusters" were identified for the three profiles when the entire beach control area (V_T) is used (colour dots, Figure 3c-e). We use the word cluster to indicate periods in time when the beach adjustment is associated with a particular trend (steepening interval), distinct from the translation (net erosion) that occurs between clusters. Each cluster has numbered events of notable change that represent the date when the cluster initially appeared, the most extreme migration event, and the date of the last observation before the system shifted to a different cluster (Figure 3c-d). By analysing the overall alignment

of the clusters and the steps between each cluster (Figure 3c-e, left panels), the behaviour of the beach can be interpreted based on the modes defined in panel a. Only profile changes (Figure 4 and 5) for Profiles 1 and 3 are shown, since the centroid analysis displayed different chronologies (Figure 3c-e, right panels) and beach behaviour for these two profiles (Profiles 1 and 2 are characterized by very similar dynamics). Figure 3c-d (left panels) show that all three profiles never return to an earlier cluster (steepening interval), but rather shift diagonally towards quadrant IV (i.e., retreat), indicating that whole profile is losing sediment. This separation between clusters in the direction of the quadrant IV was more evident for Profile 3, which experienced the largest loss of sediments (Figure 6).

The primarily diagonal movement towards the quadrant I within each cluster indicates the dominance of steeping, while the changes from the last date of one cluster to the first date of the following one, mainly correspond to steps towards the quadrant III (Profiles 1 and 2), indicating significant flattening events (Figure 4d, g). Nonetheless, during the first large dune erosion event attributed to the March 10, 2008 “Johanna” storm, Profile 3 showed a movement towards the quadrant IV, indicating beach retreat (Figure 5d).

The first cluster in all three profiles (beige dots) corresponds to the period from the beginning of the measurements (2004/07, see label 0) to the last date before a shift to a different cluster (2008/02, see label 2). During this period, the three profiles mainly experience profile steepening, (e.g., migration towards quadrant I, from label 0 to label 1), reaching the maximum steepness (left panels Figures 3c-e) for Profiles 1 and 2 in 2007/11 (Figure 4b) and in 2006/11 for Profile 3 (Figure 5b). Other beach movements within the clusters, due to seasonal-annual variations are observed (see dot with label 2 in Figure 3c-e, Figure 4c, and Figure 5c), although with less pronounced effects on the beach behaviour. On March 10, 2008, the high energy storm

404 Johanna hit the French Atlantic coast causing significant dune face erosion (Suanez et al., 2012;
405 Suanez & Cariolet, 2010), inducing beach changes associated with a new cluster (red dots,
406 Figure 3c-e, left panels).
407

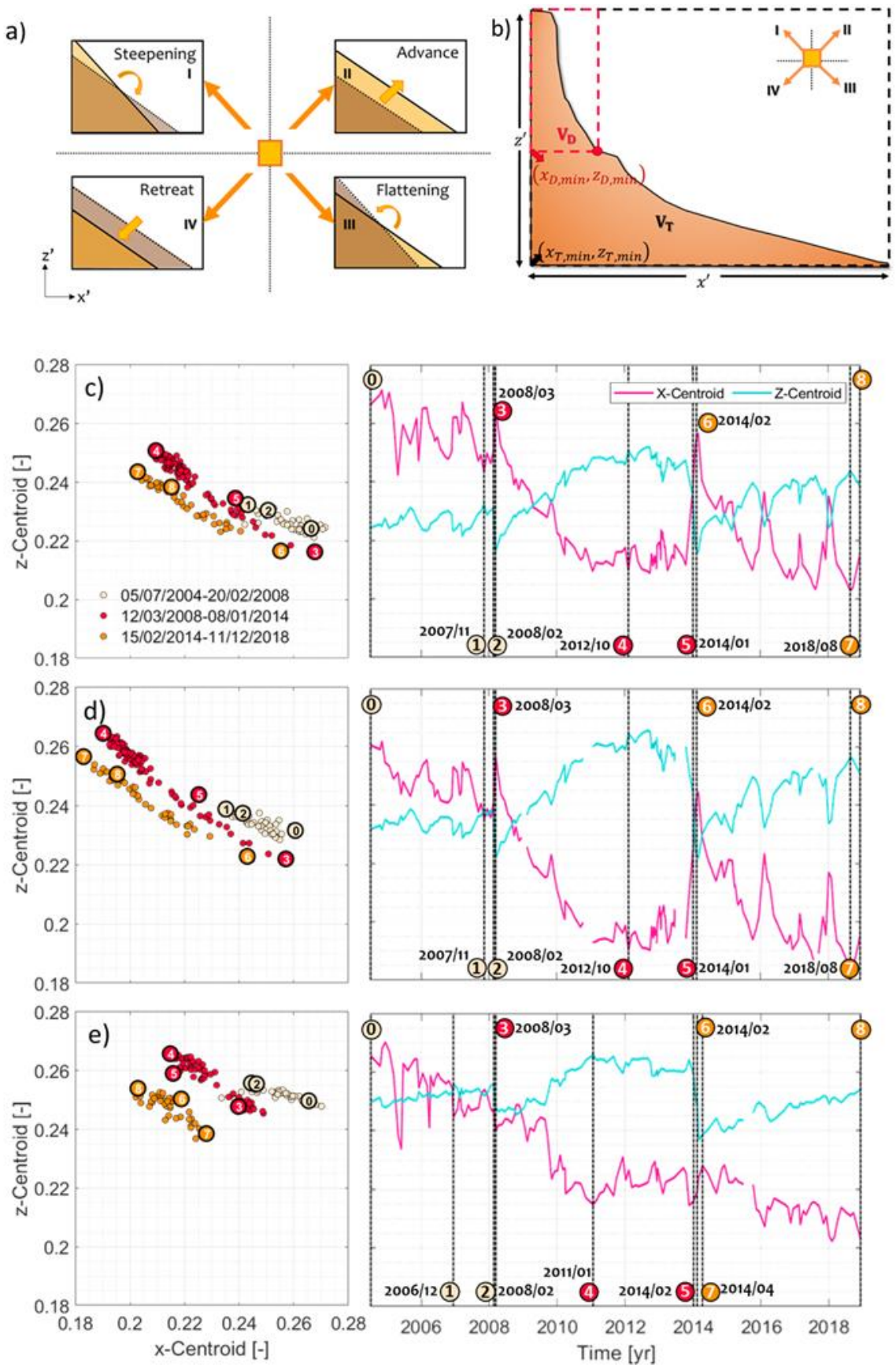
a)
Steepening
I
Advance
II
Retreat
IV
Flattening
III
z'
x'
b)
I
II
III
IV
z'
V_D
$(x_{D,min}, z_{D,min})$
V_T
$(x_{T,min}, z_{T,min})$
x'
c)
d)
e)
z-Centroid [-]
x-Centroid [-]
05/07/2004-20/02/2008
12/03/2008-08/01/2014
15/02/2014-11/12/2018
X-Centroid
Z-Centroid
2008/03
2014/02
2007/11
2008/02
2012/10
2014/01
2018/08
2011/01
2006/12
2014/04
Time [yr]

408

Figure 3. Beach migration analysis. a) Diagram of the four primary modes of beach change inferred from the centroid movement. The dotted black line represents the initial beach state (yellow square), while the solid black line represents the subsequent beach state. The four quadrants are used in the interpretation to indicate the x- and z-centroid movement between each survey; b) Control areas for the beach volume and centroid computations: Total volume $\boldsymbol{V_T}$ (black dashed square) and dune volume $\boldsymbol{V_D}$ (red dashed square), where the red dot represents the initial dune toe, modified from Townend (2018); c) to e) Centroid analysis for profiles 1, 2 and 3, respectively. Left: Non-dimensional centroid maps in the x'z' vertical plane. The colours represent the three different clusters identified through the centroid analysis. Right: Centroid evolution in time (corresponding dates in right panels).

A pronounced flattening (quadrant III migration, label 2 to 3, Figure 3c,d, left panels) was observed for Profiles 1 and 2 (Figure 4d), and a retreat (quadrant IV) for Profile 3 (Figure 3e, Figure 5d). However, after the storm, the three profiles returned to showing primarily profile steepening (in the quadrant I direction, label 3 to label 4). The maximum steepening for Profiles 1 and 2 was observed on 2012/10 (label 4, Figure 3c, d and Figure 4e) and on 2011/01 for Profile 3 (label 4, Figure 3e and Figure 5e). As in the first cluster, different migration modes such as flattening, are observed before a change to a new cluster (label 4 to 5, Figure 3c-f, Figure 4f, and Figure 5f). Most of the flattening was caused by a sequence of storms during the 2013/2014 winter that eroded the lower part of the dune, without causing a change in the cluster. From the sequence of storms experienced that winter, only the storm on February 1-2, 2014, during which the dune face was strongly eroded, generated a change to a new the cluster (yellow dots in left panels, Figure 3c-e). Behaviour within this cluster was different for Profile 3, which experienced flattening (label 6 to 7, Figure 3d and Figure 5h) and dune face erosion, contrary to Profiles 1 and

2. It is plausible that Profiles 1 and 2 were already highly eroded due to the February storm, which did not cause a significant erosion in Profile 3.

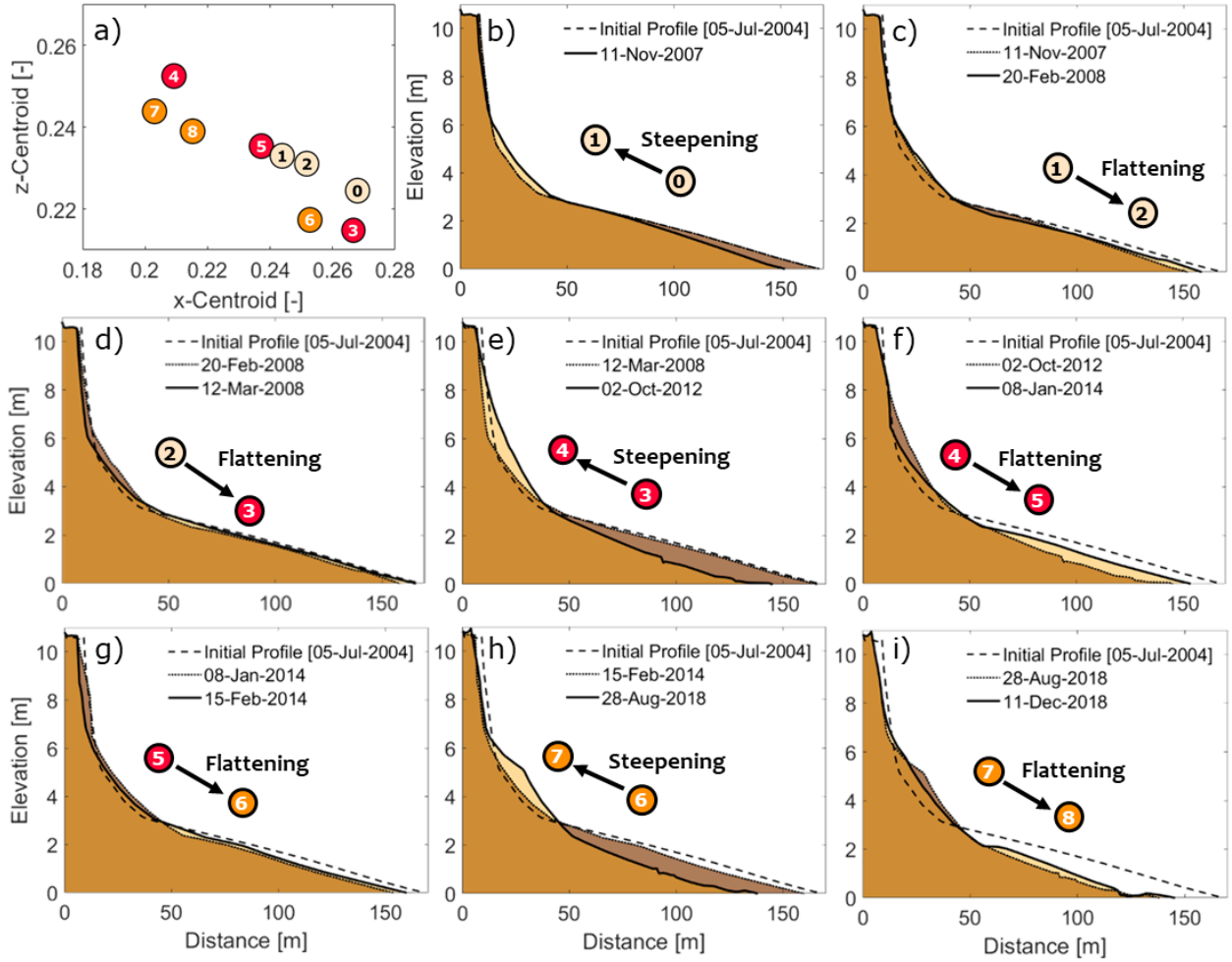

Figure 4. Beach changes in Profile 1 corresponding to the non-dimensional centroid analysis in Figure 3c. (a) non-dimensional centroid map showing the most significant changes only; b-i) Dune and beach face profiles for each event.

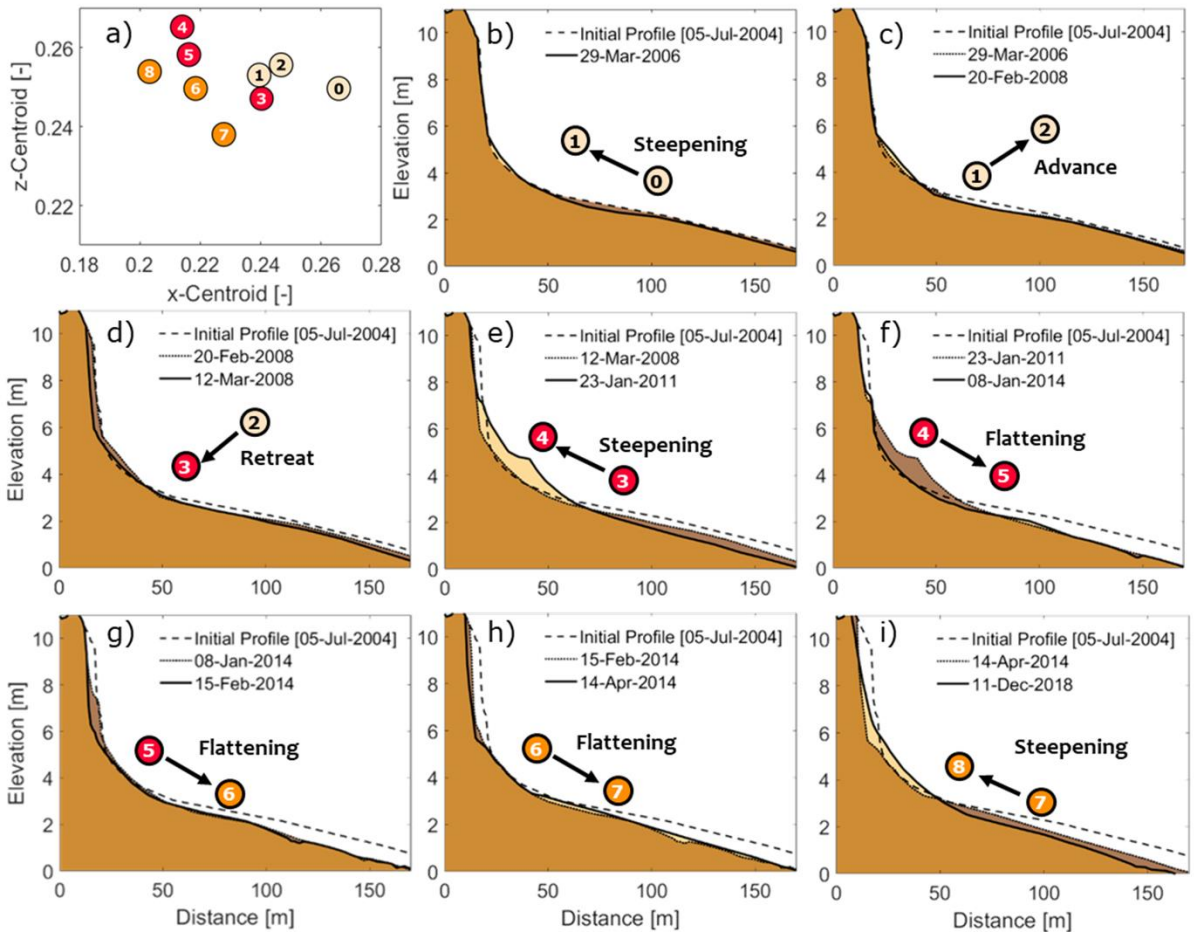

Figure 5. Same caption as Figure 4 but for Profile 3.

The right panels in Figure 3c-e show the x (red lines) and z (yellow lines) centroid evolution over time. The two large erosion events and subsequent recovery of the dune due to the erosion of the intertidal beach changed the beach dynamic. As observed in the left panels, Profiles 1 and 2 show similar behaviour. Whilst we highlight distinct phases of beach migration mode for the entire beach (V_T), Figure 3c-d, right panels, show that the x and z-centroid, plotted to the same non-dimensional scale, are not always mirrored traces of each other. When they are this implies the dominance of steepening or flattening, However, when the change of both centroids is positive or negative, this implies advance or retreat, respectively. Results show periods of predominant translation modes

448 (retreat/advance) or rotation modes (steepening/flattening), although there are also times when a
449 translation and a rotation mode occur simultaneously.

450 The total beach volume (dune and intertidal zone, black line, Figure 6, panels a, c and e)
451 during the measurement period showed a decreasing long-term trend for the three profiles, in
452 agreement with the migration between clusters towards the quadrant IV (Figure 3,c-e). Along
453 Profiles 1 and 2, the dune had stages of complete recovery when compared with the initial profile
454 (as seen by comparing the dashed line and dotted line in Figure 4f, and as seen by the dashed
455 gray lines in Figure 6). However, the dune in Profile 3 showed a significant loss in volume when
456 compared with the initial profile. Changes in the dune, upper tidal beach, and total volumes also
457 show different behaviour for Profile 3. For instance, the two large dune erosion events (labels 3
458 and 6) resulted in a slight increase in the total sediment volume for Profiles 1 and 2, while Profile
459 3 showed a large volume decrease. This might be explained by the importance of cross-shore
460 sediment exchanges between the inter-tidal beach and dune (and vice versa) for Profiles 1 and 2.
461 A stronger annual cycle is observed in Profile 3, although the long-term retreat trend dominated
462 the overall profile change (See Figure 6e). The long-term trend is likely to be due to the
463 longshore sediment transport towards the west (Suanez et al., 2012) due to wave refraction
464 caused by small islands and reefs (see Figure 2b in Suanez et al., 2012).

465 Also, changes in volume along Profile 3 display a clear erosional trend with a
466 superimposed strong annual cycle. Profiles 1 and 2, only showed an annual cycle after the
467 February 1-2, 2014 storm event. The different beach migration modes are identified in each time
468 series, showing variable responses as a function of time (colours, Figure 6 a, c, and e, with
469 legend in e). The histograms in Figure 6b, d and f show that the rotation modes, steepening (ST)
470 and flattening (FT), are predominant. However, as explained previously, steepening and

flattening modes can occur simultaneously with translation modes (advance and retreat), as observed at Vougot Beach. The dune volume changes show a large dune recovery (2008-2014) for Profiles 1 and 2, while the volume increase in Profile 3 was smaller (dashed grey line, Figure 6a, c, and e).

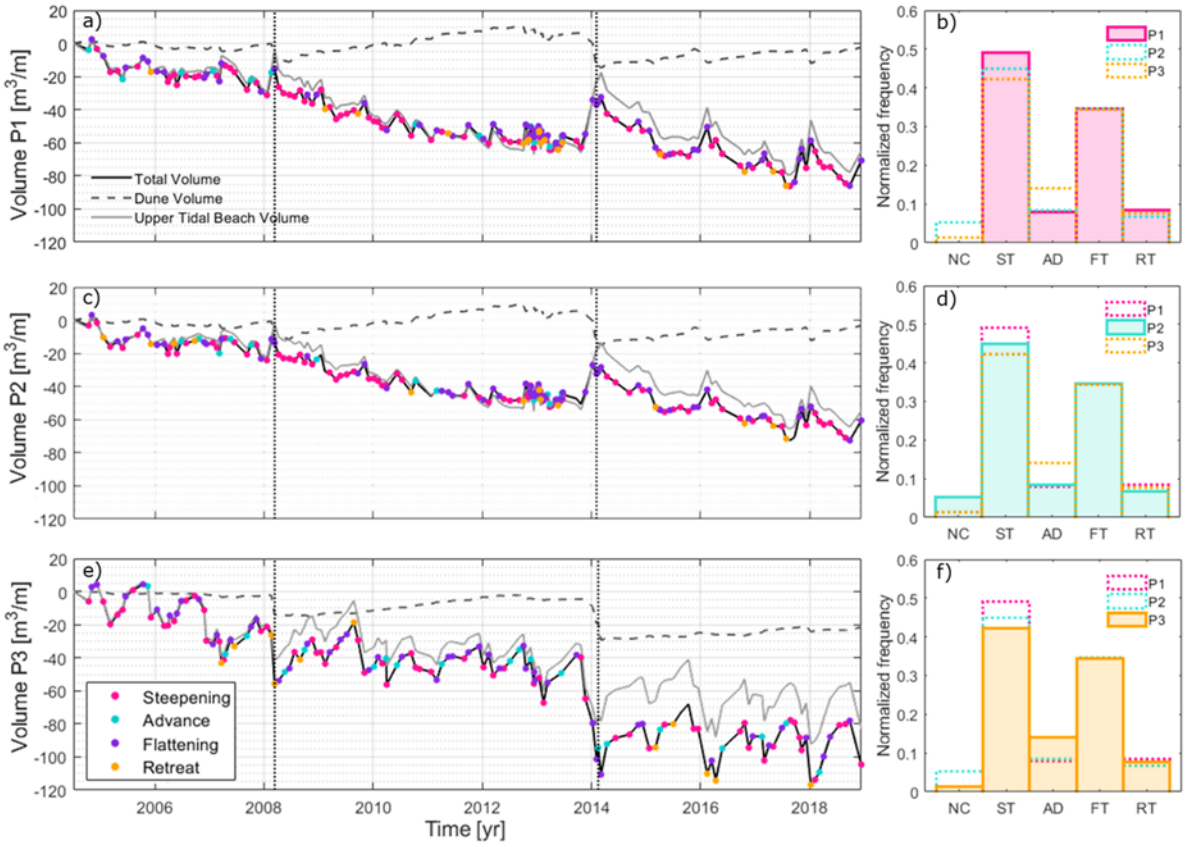

Figure 6. Beach/Dune volumes and different migrations modes in time. a), c) and e) Volume changes for the three profiles: total volume (black line), dune volume (dashed grey line), and upper intertidal beach volume (solid grey line). The coloured dots show the occurrence of different migration modes (identified in the legend) over time. b), d) and f) Histograms of the

480 different migration modes for each profile: no change (NC), steepening (ST), advance (AD),
481 flattening (FT), and retreat (RT).

482 The dune control area and volume (red square, Figure 3b) are small when compared with
483 the total beach and intertidal volumes. Therefore, the centroid analysis was carried out for the
484 dune and intertidal beach separately to better understand their respective dynamics. In this case,
485 the analysis was performed preserving the dimensions (Equations 2-4), with the aim to observe
486 the magnitude of the centroid displacement (see axes Figure 7). The dune displays opposing
487 behaviour to the total beach migration modes, i.e., when the lower dune is eroded (steepening)
488 the centroid analysis for the total beach control area shows flattening (Figure 7, middle and left
489 panels). The clusters in Profile 3 shift to the quadrant IV, much the same as the total beach,
490 implying net retreat. In contrast, profiles 1 and 2 exhibit a form of recovery over the 3
491 flattening/steepening episodes. This is in broad agreement with the volume analysis for the dune
492 observed in Figure 4a, c (sediment recovery) and e (loss of sediment).

493 When only the intertidal beach is analysed, the cluster separation is less evident for Profiles 1
494 and 2, displaying mainly steepening (in the direction of the quadrant I). This may be explained
495 by the upper part of the intertidal beach gaining sediment from the dune after the two big storm
496 events, as shown in the volume analysis (Figure 6a, c, solid grey line), while the lower part of the
497 beach loses sediment. In contrast, Profile 3 showed clearer cluster separation implying intertidal
498 beach retreat (quadrant IV trend), in agreement with the loss of sediment in this zone after the
499 two large storms (Figure 6e, solid grey line). These findings are consistent with Suanez et al.
500 (2012).

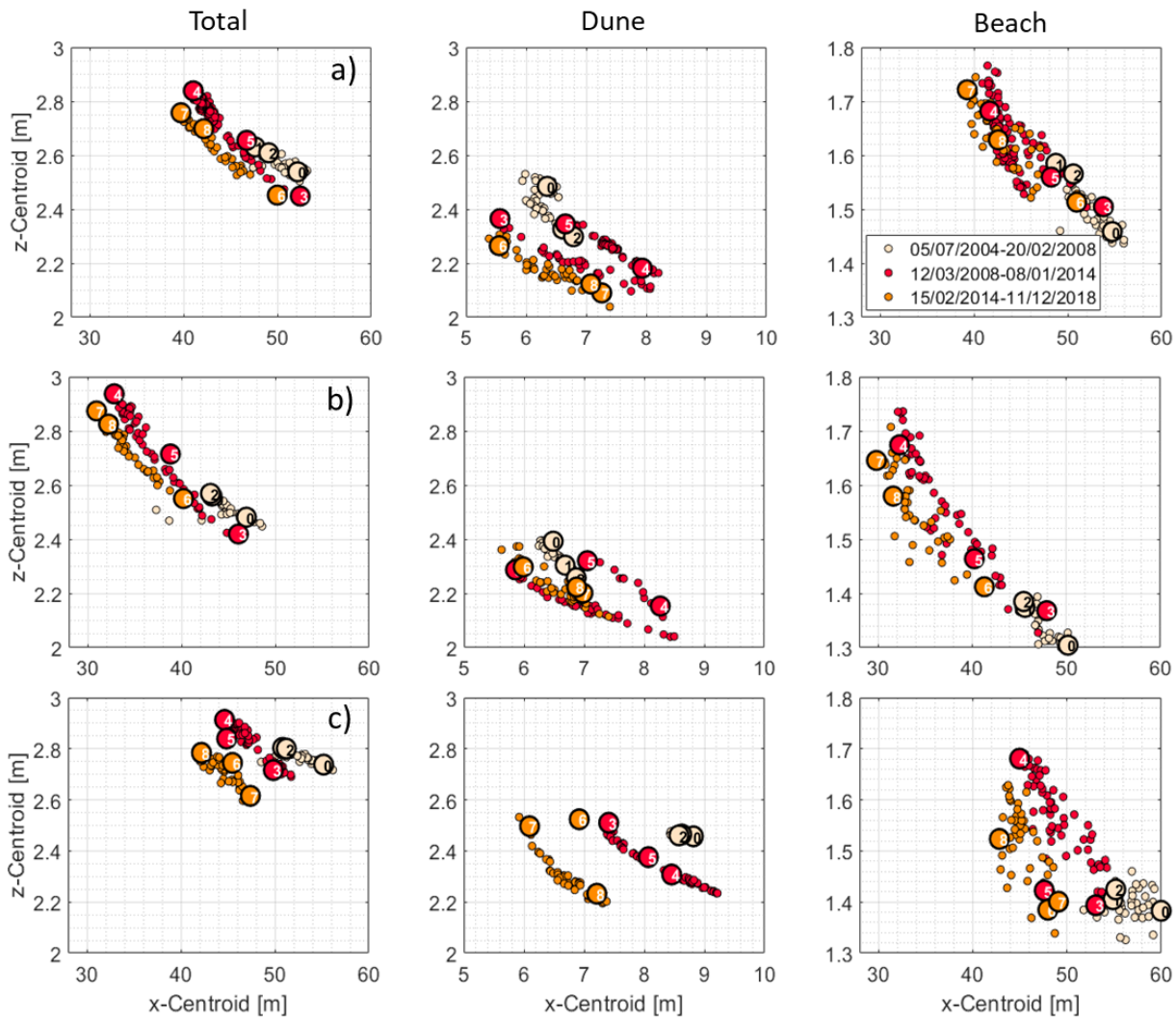

Figure 7. Dimensional centroid maps in the x'z' vertical plane for a) Profile 1; b) Profile 2: c) Profile 3. The colours represent the three different clusters identified through the centroid analysis: (left panels) for the total control area ($\boldsymbol{V_T}$), same as Figure 3c-e; (middle panels) for the dune control area ($\boldsymbol{V_D}$); and (right panels) for the intertidal beach control area.

3.2 Shoreline evolution and time-scales

The centroid analysis shows a dominant steepening trend of the beach during the studied period, with contour elevations retreating strongly along the lower part of the beach and

advancing along the upper part of the beach (as seen in Figure1, left panels and Figure 8c and f lower panels). The analysis also showed that the steepening process was interrupted by a strong flattening process during two large dune erosion events in 2008 and 2014, resetting the changes in the shoreline position with a sudden shoreline advance in the lower part of the beach and retreat in the upper part of the beach, especially for Profiles 1 and 2. With the aim of analysing and predicting shoreline changes at Vougot Beach, a recently developed modelling approach SPADS (Montaño et al. 2021) was applied. This approach was tested previously at two cross-shore dominated beaches where dune face dynamics contributed minimally to shoreline evolution, which is in contrast to this site.

For this analysis, the intertidal beaches of Profiles 1 and 3 were divided in three sections: lower, middle (a zone around the nodal/inflection point) and upper, since the three selected areas show distinctive behaviour (Figure 1f). Figure 8 shows the shoreline trends and the three primary time-scales (IMFs) identified with the CEEMD method (yellow lines, right axis) for both profiles, where the coloured dots (labels 3 and 6) indicate the two large dune erosion events. The upper part of the beach in Profile 1 (4.5 m, Figure 8a) is dominated by a long-term accretion trend, which explains up to 49% of the shoreline variance. However, the lower part of the beach showed a strong erosion trend with an explained variance (E.V) of about 48% (-0.5 m, column Figure 8c). Near the ‘inflection point’ (3m, column Figure 8b), the long-term trend only explained about 9% of the shoreline variance. The behaviour of the trend at the three elevations is in agreement with the dominant steepening mode revealed by the centroid analysis (with significant trends in the upper and lower beach and nearly no trend near the inflection point). In the middle part of the beach, a 2005-day oscillation, which is on the order of the period between the two large dune erosion events (2168 days), had the highest E.V (32%). At all three

elevations, an oscillation of about 3400 days had an important E.V (12% to 28%), in which peaks and valleys are in phase with the maxima of shoreline advances/retreat. In the upper and lower parts of the beach, oscillations with similar time-scales as the duration of the clusters (1224 days, cluster 1; 1665 days, cluster 2; and 1760 days, cluster 3) were also found. In the three sections of the beach, the annual time-scale explained only 13%, 6%, and 10% of the E.V, while the seasonal scale seemed to be important only in the middle part of the beach (14% E.V, not shown). An approximately bi-annual time scale was identified with E.V lower than 10% for all three elevations (not shown).

Conversely to Profile 1, for Profile 3 the upper part of the beach (4 m, Figure 8d) did not show a strong advancing long-term trend (only 9%), while the middle (2.5 m, Figure 8e) and lower parts (1.5m, Figure 8f) of the beach experience stronger long-term retreating trends compared to Profile 1 (28%, 85% of the E.V). This may be explained by the shape of the clusters in Profile 3 (Figure 3e), where the steepening mode (towards the quadrant I) was smaller compared with Profiles 1 and 2, while the retreat mode to a new cluster (towards the quadrant IV) was larger. As in Profile 1, temporal scales with a 3400-day oscillation corresponding to maximum retreat/advance of the shoreline were observed only in the upper and lower parts of the beach. For all three sections of the beach, the oscillations with time scales similar to the length of the clusters had E.V of 2% to 15%. In the upper part of beach, the annual oscillation showed a significant increase in amplitude after 2014, which was also observed for Profile 1. Also similar

552 to Profile 1, the E.V in the middle part of the beach (Figure 8e) was distributed more evenly
553 among the different time scales, with a strong E.V at the annual scale (31%).

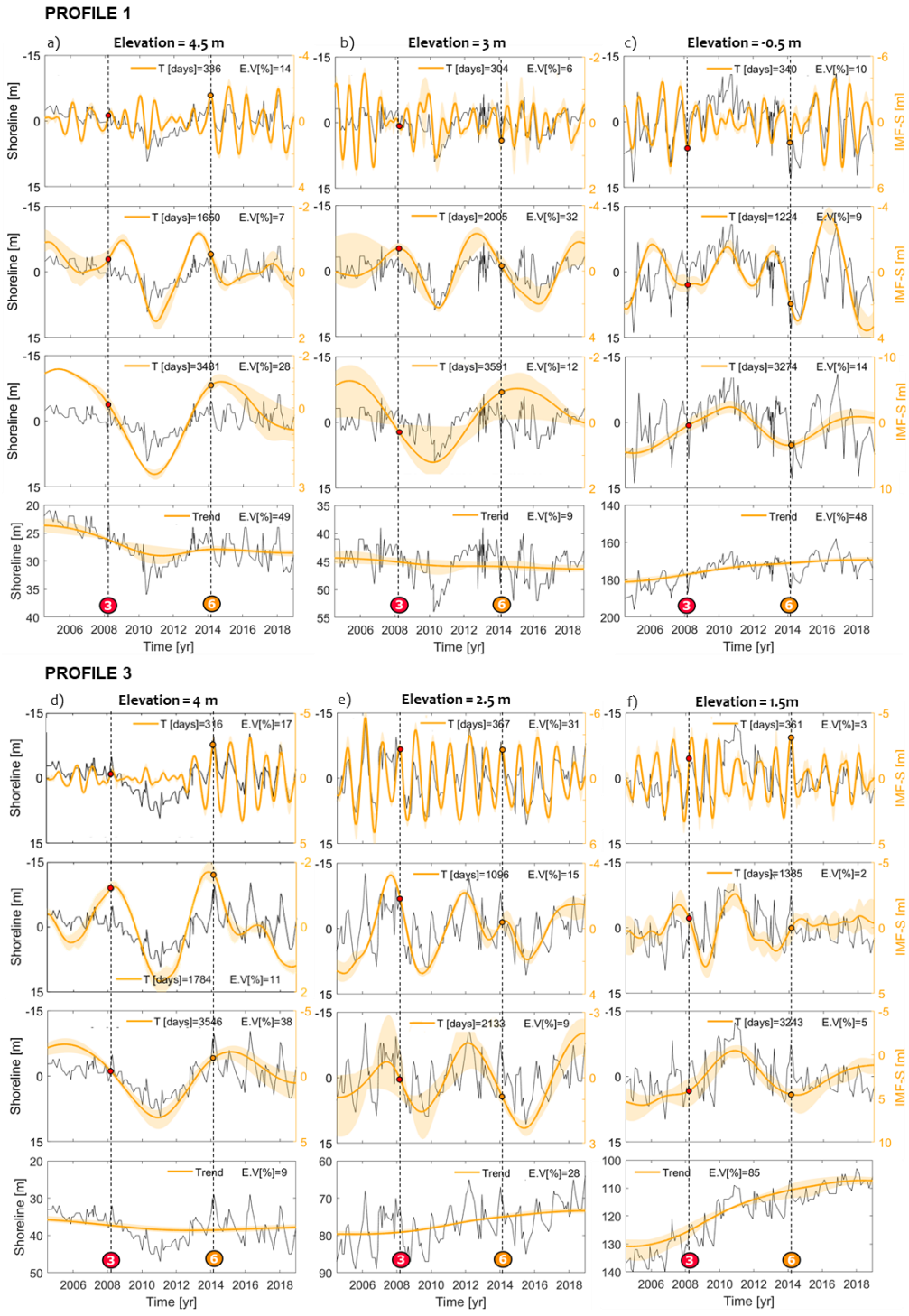

554

Figure 8. Examples of three dominant shoreline time-scales (top three rows) and the long-term trend (bottom row) identified with the CEEMD analysis for three different elevations. Profile 1 (top) columns: a) upper (4.5 m); b) middle, near the inflection point (3 m); and c) lower (-0.5 m) part of the beach; and Profile 3 (bottom) columns: d) upper (4 m); e) middle (2.5 m); and f) lower (1.5 m) part of the beach. The black line represents the detrended shoreline data (left axis), where small values of the shoreline position represent an eroded state and large values an accreted state. The yellow lines display time oscillations of the IMFs (IMF-S, right axis) after noise averaging, showing the approximate period in days of the shoreline oscillation (T) and the percentage of explained variance (% E.V). The standard deviation due to different white noise levels is represented by the shaded yellow zone. Numbers in colour represent the dates of the two large dune erosion events (vertical dashed lines).

3.3 Shoreline modelling

The shoreline change model was applied at the elevations presented in Figure 8 for Profiles 1 and 3.

3.3.1 Hindcast

The hindcast results (covering the span of the data time series) for Profile 1 (Figure 9a) and Profile 3 (Figure 9c) show that the model is capable of reproducing the contour elevation changes, with $\boldsymbol{R}^{\mathbf{2}}$ values ranging from 0.72 to 0.95. At Profile 1, the ShoreFor model performed poorly ($\boldsymbol{R}^{\mathbf{2}}$ values ranging from 0.1 to 0.53) since it only captures the long-term trend, which is not directly related to the wave forcing. At Profile 3, the ShoreFor model performs better, especially in the upper and middle part of the beach, capturing some of the annual oscillations. However, similar to Profile 1, the model coefficients are primarily controlled by the long-term

trend. This is more evident in the upper part of the beach for Profile 3 (Figure 9c, upper panel), where shoreline advance is observed between the two large dune erosion events, generating a large oscillation (38% of the E.V, Figure 8d, third panel) that is not captured by the ShoreFor model.

3.3.2 Forecast

A test of the model predictive skill was performed by training the model with 12 years of data, and then forecasting the remaining 2.5 years of shoreline evolution (gray area, Figure 9 b,d). In general, the SPADS model showed good performance when predicting the last 2.5 years of shoreline changes (yellow lines), except for the lower part of the intertidal zone of Profile 3 (Figure 9d, lower panel), where the model underestimated the long-term trend while still following the annual cycle. The ShoreFor model behaviour performed similarly (orange line) during the forecast and hindcast runs, except for lower part of the intertidal zone of Profile 1 (Figure 9b, lower panel) where, surprisingly, the model captured better the annual cycle and the long-term trend in comparison to the hindcast results (Figure 9a, lower panel).

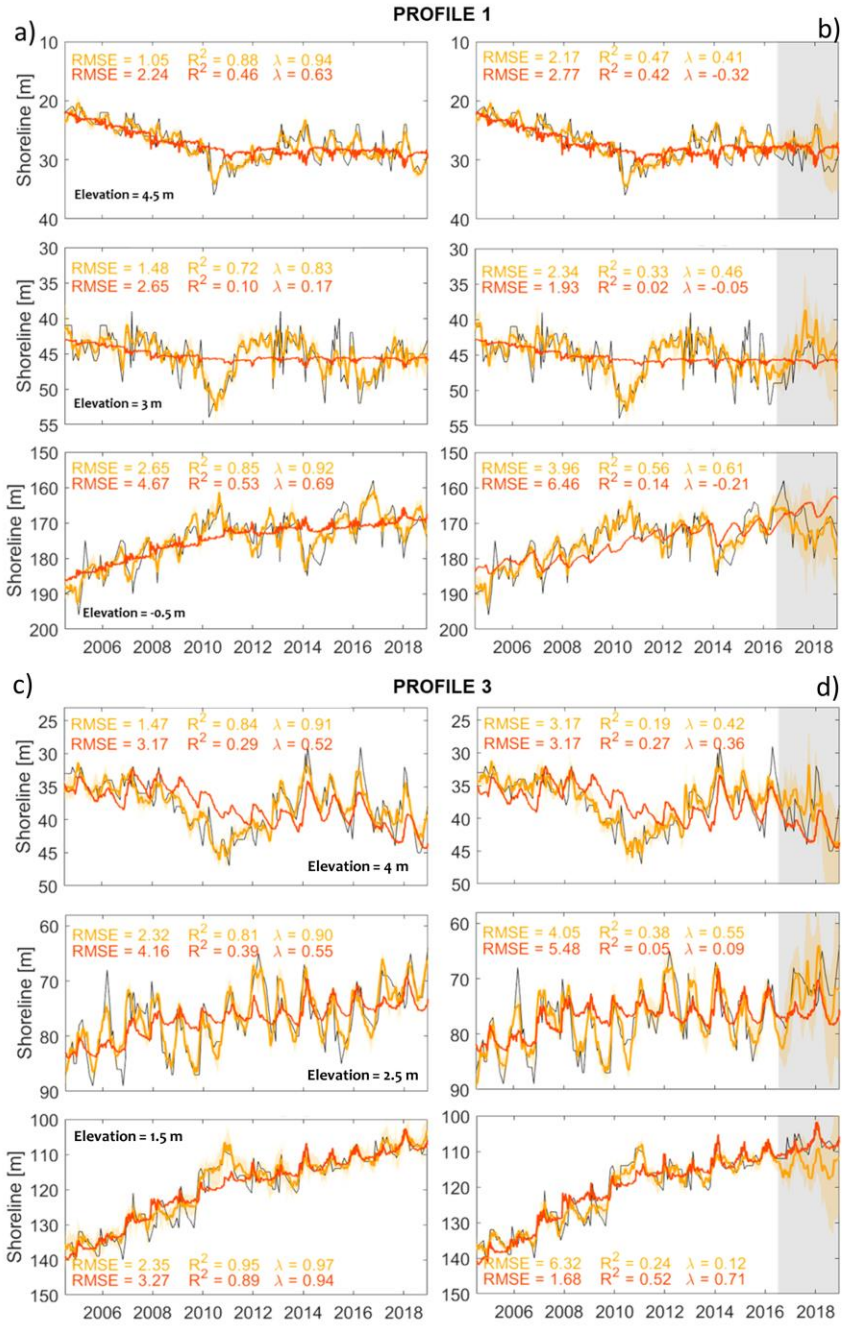

591

592 **Figure 9**. Model performance at three vertical elevations (same as shown in Figure 7) for Profile

593 1: a) hindcast; b) forecast; and Profile 3: c) hindcast; d) forecast, showing the shoreline

measurements (black lines), the SPADS model (yellow lines and metrics), the ShoreFor Model (orange lines and metrics).

4 Discussion

4.1 Beach migration modes

A centroid analysis was carried out considering both the dune and the intertidal beach volumes (scheme Figure 3b), allowing the identification of large changes in the dune-beach system. This study showed that despite the dominant beach sediment loss trend, the beach experienced different behaviour in the upper and lower parts of the intertidal zone. During the study period, the beach profile experienced mainly steepening (advances in the upper intertidal zone, and retreat in the lower intertidal zone), in which the loss of sediment in the lower part of the beach was larger than the gain of sediment in the upper part (dune and berm recovery, Figure 7), indicating an overall decrease in sediment volume along the intertidal profile. Contour elevations along the upper part of the beach showed a long-term advance trend (Figure 8a,d, bottom panels), in agreement with the dominant steepening mode. The analysis also allowed identifying differences in beach translation/rotation modes. For instance, the flattening mode only generates changes in the steepening interval (cluster) when the dune face and the upper part of the beach are eroded, redistributing large amount of sediments along the lower intertidal beach due to storm events (Figures 3 to 5). Although the flattening mode was observed frequently (Figure 6), in general, this was caused by the lower part of the dune and berm being eroded, without a large amount of sediment being redistributed in the lower intertidal zone. In agreement

with Townend and McLaren (1988) and Taylor (2004) our analysis showed that the beach might experience steepening/flattening modes in addition to a net profile retreat or advance.

Different studies have addressed beach/dune sediment exchanges based on volume analyses with the goal of classifying the beach response during storm and recovery periods (Beuzen et al., 2019; Burvingt et al., 2017; Phillips et al., 2019; Taylor, 2004). Based on volumetric changes, Burvingt et al. (2017) used hierarchical clustering to analyse beach migration modes during extreme storms at 157 beaches in England. In contrast to the centroid analysis, the volume computations for the upper and lower parts of the beach require defining a pivot point (nodal point), which is not always evident and may even change in time, making the analysis difficult. Moreover, contributions of the dune system to the beach dynamics were neglected in their analysis. Phillips et al. (2019) used a decision tree classification and described four behavioural modes of subaerial profile variability during berm recovery. However, they also neglected the dune contributions in their study. Using a Bayesian network analysis, Beuzen et al. (2019) indicated that variability in berm and dune storm erosion was controlled by morphological conditions such as exposure to incident waves, pre-storm beach sand volume, and pre-storm beach width. Similar results were found in studies of the impact of the 2013/2014 winter storms on the UK coastline, where variability in coastal storm erosion response was attributed to the coastline indentation and the associated variability in beach orientation and direction of incident wave attack (Burvingt et al., 2018; Masselink et al., 2016). In this study, in addition to the Curnic jetty influence, the differences in the beach/dune response between Profiles 1 and 2 (behaving similarly) and Profile 3 may be attributed to the profile exposure to incoming waves. As can be seen in Figure 1b, local refraction and diffraction effects likely cause

differences in the nearshore wave field, which may also explain the more evident annual volume changes observed at Profile 3 (Figure 6).

4.2 Implications for shoreline modelling

In macro-tidal environments, the wave conditions, hydrodynamic processes, and duration of exposure to these conditions depends on the elevation in the intertidal zone (Masselink & Short, 1993). Equilibrium models have been tested previously at macro and meso-tidal beaches displaying different behaviour across the intertidal zone (Castelle et al., 2014; Lemos et al., 2018). Sediment eroded from the upper intertidal zone is expected to be transported to the lower intertidal zone, much like the redistribution of sediment along the full profile of micro-tidal beaches (e.g., Winant et al., 1975; Yates et al., 2009). This study shows that when shoreline oscillations are analysed in terms of their dominant time-scales, temporal oscillations in the upper (Figure 8a) and lower (Figure 8c) part of the beach are observed to be out of phase for Profile 1. This is in agreement with the predominant steepening/flattening processes observed for this profile. This was not as evident at intra-annual time scales for Profile 3. Waves at Vougot Beach are characterized by a strong seasonal-annual signal (Figure 2g, h). Nonetheless, previous studies at Vougot Beach have found that there is no correlation between wave conditions and beach volume changes (Dodet et al., 2019). The authors argued that the beach–dune system continually lost sediment, independent of the wave conditions, due to the construction of the Curnic jetty preventing the sediment fluxes coming from the east (Suanez et al., 2010). Therefore, the long-term trend of chronic erosion is not directly related to wave forcing, but to sediment scarcity, and the longshore current dynamics. However, in the short-term a significant cross-correlation was observed between beach volume changes and Extreme Water Levels (Suanez et al., 2015). However, Figure 6c shows that volume changes along Profile 3 display a

strong annual cycle, and even Profiles 1 and 2 also display a strong annual cycle after the highly energetic 2013/2014 winter. The analysis presented here also allowed identifying the different time-scales of shoreline changes and the drivers that dominate the observed changes, showing that the annual scale has an important role in explaining changes at certain cross-shore elevations (Figure 8). This could explain why the ShoreFor model had a better performance in the profiles where the annual scale was important.

Observations of large sediment exchanges between the beach and the dune showed that dune contributions play an important role in shoreline evolution. In particular, most beach-only shoreline change models predict shoreline retreat during large storm events, while the opposite may be true if dune erosion contributes sediment to the beach, causing shoreline advance. The developed method showed that some of the oscillations with higher explained variance than the annual time-scale were related to dune morphodynamics and accounted for both the erosion events and the subsequent dune recovery phase (T~3400 days), which was associated with a period when no extreme storms and water levels occurred, allowing the upper beach and dune to recover. We notice that the oscillations at this time-scale are entirely dependent on the occurrence of major storms and likely vary for different sites based on the overall wave and/or atmospheric climate. This highlights the importance of linking dune and beach interactions to improve shoreline predictions. The relevance of this time-scale was different among the different profiles and contour elevations, in particular having a more important role along the upper part of the beach. Although the proposed modelling approach does not directly consider dune processes, it is able to reproduce shoreline changes related to dune sediment contributions. Although the proposed modelling approach does not directly consider dune processes, it is still able to simulate shoreline changes related to dune sediment contributions. The model makes use of the

682 SLP field and gradients, which contain information about the mean sea level fluctuations and
683 large atmospheric patterns (Montaño et al., 2021, Camus et al., 2004a, b) such as the North
684 Atlantic Oscillation index, which have been related to dune erosion/accretion events at Vougot
685 (Suanez et al. 2015) and the West Europe Pressure Anomaly (Castelle et al. 2017) which have
686 been found to control beach evolution in the latitudes of Brittany and southern England (Stéphan
687 et al., 2018, Dodet et al., 2019; Scott et al., 2020). Therefore, including SPL fields and their
688 gradient as drivers in the model becomes a surrogate for processes that cause dune erosion.”

689 The majority of shoreline change models (excluding detailed process-based models such
690 as XBeach) are not able to take into account the beach/dune sediment exchanges. For example,
691 the ShoreFor model does not account for these interactions, so the observed poor skill on beach
692 where interactions with dunes are important is not surprising. Interestingly, ShoreFor
693 demonstrates better performance during the forecast period than when the whole dataset was
694 used for calibration for Profile 1 (Figures 8b, bottom panel). The reduced skill during the
695 hindcast is likely due to the shoreline being characterized by an E.V that is distributed similarly
696 among the different IMFs (Figure 8c). Overall, ShoreFor tries to optimize a single parameter to
697 account for all time-scales (and their interactions), whereas the newly proposed approach treats
698 each time-scale separately and is hence able to reproduce better different physical processes
699 acting on shorter and longer time-scales.

700 A variety of models have been proposed to predict dune and beach evolution, but only a
701 limited number of them predict the effects of beach and dune interactions on multiple time-scales
702 (Antolínez et al., 2019; Hanson et al., 2010; Larson et al., 2016; Palalane et al., 2016). One of the
703 limitations of these models is that they are based on assuming a schematized profile shape,
704 usually with a fixed berm, neglecting seasonal changes. In addition, in some of these models,

sediments transported to the beach from dune erosion are redistributed throughout the whole profile instantaneously, neglecting lags in the distribution to the lower parts of the shoreface profile (Antolínez et al., 2019; Suanez et al., 2012). The analysis presented here indicates that the shoreline response due to sediment contributions from dunes is strongly dependent on the contour elevation (Figures 8), a feature that numerical models will need to to address.

Another complication for modelling dune-beach interactions is that different drivers control both the spatial extent and temporal response of the beach (Morton et al., 1994; Phillips et al., 2019). The upper part of the beach is mainly controlled by wave action and the antecedent morphology (Davidson et al., 2013; Yates et al., 2009) while dune erosion has been found to be the combined result of wave action and total water levels (Kriebel & Dean, 1985; Larson et al., 2004; Vellinga, 1982). Furthermore, patterns of berm crest formation and vertical growth were found to be primarily governed by neap-spring tide variations in total water levels (Phillips et al., 2019). The current model suggests that the sediment contribution to shoreline changes due to dune erosion events (e.g., T 3400 days), which accounts for the 28% and 38% of the E.V in the upper part of the intertidal zone for Profiles 1 and 3, are indirectly taken into account.

5 Conclusions

Almost 15 years of intertidal beach/dune profile measurements at Vougot Beach were analysed to study the influence of the dune system on shoreline changes and the implications for shoreline modelling and prediction. Three different cross-shore profiles that display long-term erosion were first analysed using a centroid analysis. The separation between the three identified clusters in the quadrant IV direction as a result of retreat was more evident for Profile 3. The centroid analysis also identified differences in the beach response for the upper and lower parts

of the beach, showing long-term steepening trends (in the direction of the quadrant I). Nonetheless, two large dune erosion events had significant impacts on each profile (migration from one cluster to the other) by flattening the beach, temporarily slowing down the retreat.

The CEEMD analysis allowed identifying the main time-scales of the observed shoreline changes, showing that a large percentage of the explained variance along the upper intertidal beach was related to time-scales associated with the two large dune erosion events and the subsequent recovery phases. In contrast, the lower part of the beach was dominated by a long-term erosion trend. For the profile least influenced by the jetty (Profile 3) the annual scale contributed significantly to the shoreline explained variance. However, the other two profiles (Profiles 1 and 2) also showed an increase in the importance of the annual cycle signal after the 2013/2014 stormy winter, showing the importance of models that are able to capture the non-stationarity of shoreline evolution processes. These findings provide useful insight to understand that in addition to the expected seasonal-annual shoreline changes caused by incident wave variability or long-term changes associated with longshore sediment transport, other time-scales of changes may co-exist and have significant impacts on shoreline changes. As a result, this modelling approach was able to reproduce well shoreline changes at Vougot Beach, including interactions with the dunes, where traditional equilibrium models have displayed poor skill. By taking into account the dune-beach interaction, the model is able to reproduce the time-scales related to the erosion and recovery of the dunes with a commensurate adjustment (e.g. rotation or translation) in the beach profile. The dune-beach interaction is critical for understanding the behavior of the beach system and the impact of the dunes on the shoreline position. We therefore contend that by capturing the dominant time-scales in the forcing events and subsequent responses and mapping these using a centroid analysis provide sufficient insight to enable the

observed changes to be satisfactorily explained. Overall, this methodology helps to improve understanding of beach-dune interactions, and even more generally, prediction horizons at beaches where a variety of processes operate, and traditional approaches fail.

Acknowledgements

This work was supported by ISblue project, Interdisciplinary graduate school for the blue planet (ANR-17-EURE-0015) and co-funded by a grant from the French government under the program "Investissements d'Avenir", which funded my research stay at the Laboratoire Geosciences Ocean (LGO UMR 6538 CNRS) - Université de Bretagne Occidentale, and the Laboratoire d'Hydraulique Saint-Venant (LHSV) - Université de Paris-Est. The survey of the Vougot beach is realized in the framework of the french « Service National d'Observation » (SNO) DYNALIT labelled by the Institut National des Sciences de l'Univers (INSU) and co-funded by the CNRS (Centre National de la Recherche Scientifique). Vougot data are available via the INDIGEO WEB platform (https://portail.indigeo.fr/geonetwork/srv/fre/catalog.search#/metadata/c120a3fe-9341-4bb3-b58b-1be6ba1deb99). Serge Suanez , Emmanuel Blaise , Jean-Marie Cariolet , Laurence David (2016). Données pluri-décennales de suivi de profils de la plage/dune du Vougot à Guissény (Finistère, France).

References

Antolínez, J. A. A., Méndez, F. J., Anderson, D., & Ruggiero, P. (2019). Predicting Climate-Driven Coastlines With a Simple and Efficient Multiscale Model. *Journal of Geophysical Research: Earth Surface*, *124*, 1596–1624. https://doi.org/10.1029/2018JF004790

Ashton, A., Murray, A. B., & Arnault, O. (2001). Formation of coastline features by large-scale

771 instabilities induced by high-angle waves. *Letters to Nature*, *414*(November), 1–6.

772 Barnard, P. L., Short, A. D., Harley, M. D., Splinter, K. D., Vitousek, S., Turner, I. L., et al.
773 (2015). Coastal vulnerability across the Pacific dominated by El Niño/Southern Oscillation.
774 *Nature Geoscience*, *8*(10), 801–807. https://doi.org/10.1038/ngeo2539

775 Beuzen, T., Harley, M. D., Splinter, K. D., & Turner, I. L. (2019). Controls of Variability in
776 Berm and Dune Storm Erosion Journal of Geophysical Research : Earth Surface. *Journal of*
777 *Geophysical Research: Earth Surface*, *124*, 2647–2665.
778 https://doi.org/10.1029/2019JF005184

779 Blaise, E., Suanez, S., Stephan, P., Fichaut, B., David, L., Cuq, V., et al. (2015). Bilan des
780 tempêtes de l'hiver 2013-2014 sur la dynamique de recul du trait de côte en Bretagne.
781 *Géomorphologie : Relief, Processus, Environnement*, *21*(3), 267–292.
782 https://doi.org/10.4000/geomorphologie.11104

783 Blossier, B., Bryan, K. R., Daly, C. J., & Winter, C. (2017). Shore and bar cross-shore migration
784 , rotation , and breathing processes at an embayed beach. *Journal of Geophysical Research:*
785 *Earth Surface*, *122*, 1745–1770. https://doi.org/10.1002/2017JF004227

786 Boak, E. H., & Turner, I. L. (2005). Shoreline Definition and Detection: A Review. *Journal of*
787 *Coastal Research*, *214*(214), 688–703. https://doi.org/10.2112/03-0071.1

788 Boudière, E., Maisondieu, C., Ardhuin, F., Accensi, M., Pineau-Guillou, L., & Lepesqueur, J.
789 (2013). A suitable metocean hindcast database for the design of Marine energy converters.
790 *International Journal of Marine Energy*, *3–4*, 40–52.
791 https://doi.org/10.1016/j.ijome.2013.11.010

792 Bruun. (1962). Sea-Level Rise as a Cause of Shore Erosion. *Journal of the Waterways and*
793 *Harbors Division*, *88*(1), 117–132.

794 Bruun, P. (1988). The Bruun Rule of Erosion by Sea-Level Rise : A Discussion on Large-Scale
795 Two- and Three- Dimensional. *Journal of Coastal Research*, *4*(4), 627–648.

796 Burvingt, O., Masselink, G., Russell, P., & Scott, T. (2017). Classification of beach response to
797 extreme storms. *Geomorphology*, *295*, 722–737.
798 https://doi.org/10.1016/j.geomorph.2017.07.022

799 Burvingt, O., Masselink, G., Scott, T., Davidson, M., & Russell, P. (2018a). Climate forcing of
800 regionally-coherent extreme storm impact and recovery on embayed beaches. *Marine*
801 *Geology*, *401*(April), 112–128. https://doi.org/10.1016/j.margeo.2018.04.004

802 Burvingt, O., Masselink, G., Scott, T., Davidson, M., & Russell, P. (2018b). Climate forcing of
803 regionally-coherent extreme storm impact and recovery on embayed beaches. *Marine*
804 *Geology*, *401*(March), 112–128. https://doi.org/10.1016/j.margeo.2018.04.004

805 Callaghan, D. P., Nielsen, P., Short, A., & Ranasinghe, R. (2008). Statistical simulation of wave
806 climate and extreme beach erosion. *Coastal Engineering*, *55*(5), 375–390.
807 https://doi.org/10.1016/j.coastaleng.2007.12.003

808 Camus, P., Menendez, M., Mendez, F. J., Izaguirre, C., Espejo, A., Canovas, V., et al. (2014). A
809 weather-type statistical downscaling framework for ocean wave climate. *Journal of*
810 *Geophysical Research : Oceans*, *119*, 3909–3925. https://doi.org/10.1002/2013JC009563

811 Cariolet, J. M., & Suanez, S. (2013). Runup estimations on a macrotidal sandy beach. *Coastal*

Engineering, *74*, 11–18. https://doi.org/10.1016/j.coastaleng.2012.11.008

Castelle, B., Ruessink, B. G., Bonneton, P., Marieu, V., Bruneau, N., & Price, T. D. (2010). Coupling mechanisms in double sandbar systems . Part 1 : Patterns and physical explanation. *Earth Surface Processes and Landforms*, *486*(February), 476–486. https://doi.org/10.1002/esp.1929

Castelle, Bruno, Marieu, V., Bujan, S., Ferreira, S., Parisot, J. P., Capo, S., et al. (2014). Equilibrium shoreline modelling of a high-energy meso-macrotidal multiple-barred beach. *Marine Geology*, *347*, 85–94. https://doi.org/10.1016/j.margeo.2013.11.003

Castelle, Bruno, Marieu, V., Bujan, S., Splinter, K. D., Robinet, A., Sénéchal, N., & Ferreira, S. (2015). Impact of the winter 2013-2014 series of severe Western Europe storms on a double-barred sandy coast: Beach and dune erosion and megacusp embayments. *Geomorphology*, *238*, 135–148. https://doi.org/10.1016/j.geomorph.2015.03.006

Castelle B., Dodet G., Masselink G., Scott T. (2017). A new climate index controlling winter wave activity along the Atlantic coast of Europe: The West Europe Pressure Anomaly. *Geophysical Reserch Letters*, 44 (3), 1384-1392. DOI: 10.1002/2016GL072379

Coco, G., Senechal, N., Rejas, A., Bryan, K. R., Capo, S., Parisot, J. P., et al. (2014). Beach response to a sequence of extreme storms. *Geomorphology*, *204*, 493–501. https://doi.org/10.1016/j.geomorph.2013.08.028

Cohn, N., Ruggiero, P., de Vries, S., & Kaminsky, G. M. (2018). New Insights on Coastal Foredune Growth: The Relative Contributions of Marine and Aeolian Processes. *Geophysical Research Letters*, *45*(10), 4965–4973. https://doi.org/10.1029/2018GL077836

Conlin, M. P., Adams, P. N., Jaeger, J. M., & MacKenzie, R. (2020). Quantifying Seasonal-to-Interannual-Scale Storm Impacts on Morphology Along a Cuspate Coast With a Hybrid Empirical Orthogonal Function Approach. *Journal of Geophysical Research: Earth Surface*, *125*(12). https://doi.org/10.1029/2020JF005617

Le Cozannet, G., Bulteau, T., Castelle, B., Ranasinghe, R., Wöppelmann, G., Rohmer, J., et al. (2019). Quantifying uncertainties of sandy shoreline change projections as sea level rises. *Scientific Reports*, *9*(1), 1–11. https://doi.org/10.1038/s41598-018-37017-4

D'Anna, M., Idier, D., Castelle, B., Cozannet, G. L., & Rohmer, J. (2020). Impact of model free parameters and sea-level rise uncertainties on 20-years shoreline hindcast : the case of Truc Vert beach (SW. *Earth Surface Processes and Landforms*, *45*, 1895–1907. https://doi.org/10.1002/esp.4854

Davidson, M. A., Splinter, K. D., & Turner, I. L. (2013). A simple equilibrium model for predicting shoreline change. *Coastal Engineering*, *73*, 191–202. https://doi.org/10.1016/j.coastaleng.2012.11.002

Dissanayake, P., Brown, J., Wisse, P., & Karunarathna, H. (2015). Effects of storm clustering on beach/dune evolution. *Marine Geology*, *370*, 63–75. https://doi.org/10.1016/j.margeo.2015.10.010

Dodet, G., Castelle, B., Masselink, G., Scott, T., Davidson, M., Floc'h, F., et al. (2019). Beach recovery from extreme storm activity during the 2013–14 winter along the Atlantic coast of Europe. *Earth Surface Processes and Landforms*, *44*(1), 393–401. https://doi.org/10.1002/esp.4500

Duveiller, G., Fasbender, D., & Meroni, M. (2016). Revisiting the concept of a symmetric index of agreement for continuous datasets. *Scientific Reports, 6*(January), 1–14. https://doi.org/10.1038/srep19401

Hanson, H. (1989). Genesis-A Generalized Shoreline Change Numerical Model. *Journal of Coastal Research*, *5*(1), 1–27.

Hanson, H., Larson, M., & Kraus, N. C. (2010). Calculation of beach change under interacting cross-shore and longshore processes. *Coastal Engineering*, *57*(6), 610–619. https://doi.org/10.1016/j.coastaleng.2010.02.002

Hapke, C. J., Plant, N. G., Henderson, R. E., Schwab, W. C., & Nelson, T. R. (2016). Decoupling processes and scales of shoreline morphodynamics. *Marine Geology*, *381*, 42–53. https://doi.org/10.1016/j.margeo.2016.08.008

Hegermiller, C. A., Antolinez, J. A. A., Rueda, A., Camus, P., Perez, J., Erikson, L. H., et al. (2017). A multimodal wave spectrum-based approach for statistical downscaling of local wave climate. *Journal of Physical Oceanography*, *47*(2), 375–386. https://doi.org/10.1175/JPO-D-16-0191.1

Houser, C. (2009). Synchronization of transport and supply in beach-dune interaction. *Progress in Physical Geography*, *33*(6), 733–746. https://doi.org/10.1177/0309133309350120

Huang, N. E., Shen, Z., Long, S. R., Wu, M. C., Shih, H. H., Zheng, Q., et al. (1998). The empirical mode decomposition and the Hilbert spectrum for nonlinear and non-stationary time series analysis. *Proceedings of the Royal Society A: Mathematical, Physical and Engineering Sciences*, *454*(1971), 903–995. https://doi.org/10.1098/rspa.1998.0193

Hurst, M. D., Barkwith, A., Ellis, M. A., Thomas, C. W., & Murray, A. B. (2015). Exploring the sensitivities of crenulate bay shorelines to wave climates using a new vector-based one-line model. *Journal of Geophysical Research: Earth Surface*, *120*(12), 2586–2608. https://doi.org/10.1002/2015JF003704

Kriebel, D., & Dean, R. G. (1985). Numerical simulation of time-dependent beach and dune erosion. *Coastal Engineering*, *9*, 221–245.

Larson, M., Palalane, J., Fredriksson, C., & Hanson, H. (2016). Simulating cross-shore material exchange at decadal scale . Theory and model component validation. *Coastal Engineering*, *116*, 57–66. https://doi.org/10.1016/j.coastaleng.2016.05.009

Larson, Magnus, & Kraus, N. C. (1995). Prediction of cross-shore sediment transport at different spatial and temporal scales. *Marine Geology*, *126*(1–4), 111–127. https://doi.org/10.1016/0025-3227(95)00068-A

Larson, Magnus, Erikson, L., & Hanson, H. (2004). An analytical model to predict dune erosion due to wave impact. *Coastal Engineering*, *51*(8–9), 675–696. https://doi.org/10.1016/j.coastaleng.2004.07.003

Lemos, C., Floc'h, F., Yates, M., Le Dantec, N., Marieu, V., Hamon, K., et al. (2018). Equilibrium modeling of the beach profile on a macrotidal embayed low tide terrace beach. *Ocean Dynamics*, *68*(9), 1207–1220. https://doi.org/10.1007/s10236-018-1185-1

Ludka, B. C., Guza, R. T., O'Reilly, W. C., Merrifield, M. A., Flick, R. E., Bak, A. S., et al. (2019). Sixteen years of bathymetry and waves at San Diego beaches. *Scientific Data*, *6*(1), 161. https://doi.org/10.1038/s41597-019-0167-6

Luijendijk, A., Hagenaars, G., Ranasinghe, R., Baart, F., Donchyts, G., & Aarninkhof, S. (2018). The State of the World's Beaches. *Scientific Reports*, *8*(1), 6641. https://doi.org/10.1038/s41598-018-24630-6

Masselink, G., & Short, A. D. (1993). The effect of tide range on beach morphodynamics and morphology: a conceptual beach model. *Journal of Coastal Research*, *9*(3), 785–800.

Masselink, G., Castelle, B., Scott, T., Dodet, G., Suanez, S., Jackson, D., & Floc, F. (2016). Extreme wave activity during 2013/2014 winter and morphological impacts along the Atlantic coast of Europe. *Geophysical Research Letters*, *43*, 2135–2143. https://doi.org/10.1002/2015GL067492.Received

Masselink, Gerd, Scott, T., Poate, T., Russell, P., Davidson, M., & Conley, D. (2016). The extreme 2013/2014 winter storms: Hydrodynamic forcing and coastal response along the southwest coast of England. *Earth Surface Processes and Landforms*, *41*(3), 378–391. https://doi.org/10.1002/esp.3836

Matthews, T., Murphy, C., Wilby, R. L., & Harrigan, S. (2014). Stormiest winter on record for Ireland and UK. *Nature Climate Change*, *4*(9), 738–740. https://doi.org/10.1038/nclimate2336

Miller, J. K., & Dean, R. G. (2004). A simple new shoreline change model. *Coastal Engineering*, *51*, 531–556. https://doi.org/10.1016/j.coastaleng.2004.05.006

Montaño, J., Coco, G., Antolínez, J. A. A., Beuzen, T., Bryan, K. R., Cagigal, L., et al. (2020). Blind testing of shoreline evolution models. *Scientific Reports*, *10*(1), 1–10. https://doi.org/10.1038/s41598-020-59018-y

Montaño, J., Blossier, B., Osorio, A. F., & Winter, C. (2020). The role of frequency spread on swash dynamics. *Geo-Marine Letters*, *40*, 243–254. https://doi.org/10.1007/s00367-019-00591-1

Montaño, J., Coco, G., Cagigal, L., Mendez, F., Rueda, A., Bryan, K. R., & Harley, M. D. (2021). A Multiscale Approach to Shoreline Prediction. *Geophysical Research Letters*, *48*(1), 1–11. https://doi.org/10.1029/2020gl090587

Morton, R. A., Paine, J. G., & Gibeaut, J. C. (1994). Stages and Durations of Post-Storm Beach Recovery , Southeastern Texas Coast , U . S . *Journal of Coastal Research*, *10*(4), 884–908.

Nicholls, & Cazenave, A. (2010). Sea Level Rise and Its Impact on Coastal Zones. *Science*, *328*(2010), 1517–1520. https://doi.org/10.1126/science.1185782

Palalane, J., Fredriksson, C., Marinho, B., Larson, M., Hanson, H., & Coelho, C. (2016). Simulating cross-shore material exchange at decadal scale. Model application. *Coastal Engineering*, *116*, 26–41. https://doi.org/10.1016/j.coastaleng.2016.05.007

Pérez-Alberti, A., & Trenhaile, A. S. (2015). Clast mobility within boulder beaches over two winters in Galicia, northwestern Spain. *Geomorphology*, *248*, 411–426. https://doi.org/10.1016/j.geomorph.2015.08.001

Pérez, J., Méndez, F. J., Menéndez, M., & Losada, I. J. (2014). ESTELA : a method for evaluating the source and travel time of the wave energy reaching a local area. *Ocean Dynamics*, *64*, 1181–1191. https://doi.org/10.1007/s10236-014-0740-7

Phillips, M. S., Blenkinsopp, C. E., Splinter, K. D., Harley, M. D., & Turner, I. L. (2019). Modes

of Berm and Beachface Recovery Following Storm Reset: Observations Using a Continuously Scanning Lidar. *Journal of Geophysical Research: Earth Surface*, *124*(3), 720–736. https://doi.org/10.1029/2018JF004895

Phillips, Matthew S., Harley, M. D., Turner, I. L., Splinter, K. D., & Cox, R. J. (2017). Shoreline recovery on wave-dominated sandy coastlines: the role of sandbar morphodynamics and nearshore wave parameters. *Marine Geology*, *385*, 146–159. https://doi.org/10.1016/j.margeo.2017.01.005

Plant, N. G., & Stockdon, H. F. (2012). Probabilistic prediction of barrier-island response to hurricanes. *Journal of Geophysical Research: Earth Surface*, *117*(3), 1–17. https://doi.org/10.1029/2011JF002326

Rascle, N., & Ardhuin, F. (2013). A global wave parameter database for geophysical applications. Part 2: Model validation with improved source term parameterization. *Ocean Modelling*, *70*, 174–188. https://doi.org/10.1016/j.ocemod.2012.12.001

Robinet, A., Idier, D., Castelle, B., & Marieu, V. (2018). A reduced-complexity shoreline change model combining longshore and cross-shore processes: The LX-Shore model. *Environmental Modelling and Software*, *109*(August), 1–16. https://doi.org/10.1016/j.envsoft.2018.08.010

Rueda, A., Cagigal, L., Antolínez, J. A. A., Albuquerque, J. C., Castanedo, S., Coco, G., & Méndez, F. J. (2019). Marine climate variability based on weather patterns for a complicated island setting: The New Zealand case. *International Journal of Climatology*, *39*(3), 1777–1786. https://doi.org/10.1002/joc.5912

Ruggiero, P., Komar, P. D., McDougal, W. G., Marra, J. J., & Beach, R. A. (2001). Wave runup, extreme water levels and the erosion of properties backing beaches. *Journal of Coastal Research*, *17*(2), 407–419.

Scott, T., Masselink, G., McCarroll, R. J., Russell, P. (2020). Predicting beach rotation using multiple atmospheric indices. *Marine Geology*, 426, 106207. https://doi.org/10.1016/j.margeo.2020.106207

Senechal, N., Coco, G., Castelle, B., & Marieu, V. (2015). Storm impact on the seasonal shoreline dynamics of a meso- to macrotidal open sandy beach (Biscarrosse, France). *Geomorphology*, *228*, 448–461. https://doi.org/10.1016/j.geomorph.2014.09.025

Serafin, K. A., & Ruggiero, P. (2014). Simulating extreme total water levels using a time-dependent, extreme value approach. *Journal of Geophysical Research: Oceans*, *119*, 6305–6329. https://doi.org/10.1002/2014JC010093.Received

Soulsby, R., Sutherland, J., Brampton, A., 1999. Coastal Steepening - the UK view. TR91, Wallingford, UK.

Splinter, K. D., Turner, I. L., Davidson, M. A., Barnard, P., Castelle, B., & Oltman-Shay, J. (2014). A generalized equilibrium model for predicting daily to interannual shoreline response. *Journal of Geophysical Research: Earth Surface*, *119*(9), 1936–1958. https://doi.org/10.1002/2014JF003106

Splinter, K.D., Turner, I. L., & Davidson, M. A. (2013). How much data is enough? The importance of morphological sampling interval and duration for calibration of empirical shoreline models. *Coastal Engineering*, *77*, 14–27.

https://doi.org/10.1016/j.coastaleng.2013.02.009

Splinter, Kristen D., & Palmsten, M. L. (2012). Modeling dune response to an East Coast Low. *Marine Geology*, *329–331*, 46–57. https://doi.org/10.1016/j.margeo.2012.09.005

Stephan P., Dodet G., Tardieu I., Suanez S., David L. (2018) - Multi-decadal coastline dynamics in relation to variations in meteo-oceanic forcing in northern Brittany (Goulven Bay, France), *Geomorphology: Relief, Processes, Environment*, 24 (1), 79-102. doi: 10.4000/geomorphology.11908

Suanez, S., Blaise, E., Cariolet, J. M., & David L. (2016). Données pluri-décennales de suivi de profils de la plage/dune du Vougot à Guissény (Finistère, France).

Suanez, S, Cancouët, R., Floc'h, F., Blaise, E., Ardhuin, F., Filipot, J. F., et al. (2015). Observations and predictions of wave runup, extreme water levels, and medium-term dune erosion during storm conditions. *Journal of Marine Science and Engineering*, *3*(3), 674–698. https://doi.org/10.3390/jmse3030674

Suanez, Serge, & Cariolet, J.-M. (2010). L'action des tempêtes sur l'érosion des dunes : les enseignements de la tempête du 10 mars 2008Impact of storms on dune erosion: lessons from the 10th March 2008 storm. *Norois*, (215), 77–99. https://doi.org/10.4000/norois.3212

Suanez, Serge, Cariolet, J., & Fichaut, B. (2010). Monitoring of recent morphological changes of the dune. *Shore and Beach*, *78*, 37–47.

Suanez, Serge, Cariolet, J., Cancouët, R., Ardhuin, F., & Delacourt, C. (2012). Dune recovery after storm erosion on a high-energy beach: Vougot Beach , Brittany (France).

Geomorphology, *139–140*, 16–33. https://doi.org/10.1016/j.geomorph.2011.10.014

Suanez, Serge, Cancouët, R., Floc, F., Blaise, E., & Ardhuin, F. (2015). Observations and Predictions of Wave Runup , Extreme Water Levels , and Medium-Term Dune Erosion during, (July), 674–698. https://doi.org/10.3390/jmse3030674

Suanez, Serge, Blaise, E., Cancouët, R., & Floc'h, F. (2016). Empirical Parameterization of Wave Runup and Dune Erosion during Storm Conditions on a Natural Macrotidal Beach. *Journal of Coastal Research*, *75*(sp1), 932–936. https://doi.org/10.2112/si75-187.1

Taylor, J. A., Murdock, A. P., & Pontee, N. I. (2004). A macroscale analysis of coastal steepening around the coast of England and Wales. *Geographical Journal*, *170*(3), 179–188. https://doi.org/10.1111/j.0016-7398.2004.00119.x

Torres, M., Colominas, M. A., Schlotthauer, G., & Flandrin, P. (2011). A complete ensemble empirical mode decomposition with adaptive noise. In *2011 IEEE international conference on acoustics, speech and signal processing (ICASSP)* (pp. 4144–4147). Retrieved from http://ieeexplore.ieee.org/xpls/abs_all.jsp?arnumber=5947265

Townend, I.H., Fleming, C.A., McLaren, P., Hunter-Blair, A., 1990. A regional study of coastal morphology. *International Conference of Coastal Engineering. American Society of Civil Engineers*, pp. 2589-2602.

Townend, I. H. (2018). *CoastalTools manual*.

Turner, I. L., Harley, M. D., Short, A. D., Simmons, J. A., Bracs, M. A., Phillips, M. S., & Splinter, K. D. (2016). A multi-decade dataset of monthly beach profile surveys and inshore wave forcing at Narrabeen, Australia. *Scientific Data*, *3*, 160024.

https://doi.org/10.1038/sdata.2016.24

US Army Corps of Engineers. (1984). *Shore protection manual*. https://doi.org/doi.org/10.5962/bhl.title.47829

Vellinga, P. (1982). Beach and Dune Erosion During Storm Surges. *Coastal Engineering*, *6*, 361–387.

Villamarin, B. C. (2017). *Beach Cross-shore dynamics : Applicability of Equilibrium Shoreline models*. University of Southampton.

Vitousek, S., Barnard, P. L., Limber, P., Erikson, L., & Cole, B. (2017a). A model integrating longshore and cross-shore processes for predicting long-term shoreline response to climate change. *Journal of Geophysical Research: Earth Surface*, 1–25. https://doi.org/10.1002/2016JF004065

Vitousek, S., Barnard, P. L., Limber, P., Erikson, L., & Cole, B. (2017b). A model integrating longshore and cross-shore processes for predicting long-term shoreline response to climate change. *Journal of Geophysical Research: Earth Surface*, 1–25. https://doi.org/10.1002/2016JF004065

Vos, K., Harley, M. D., Splinter, K. D., Simmons, J. A., & Turner, I. L. (2019). Sub-annual to multi-decadal shoreline variability from publicly available satellite imagery. *Coastal Engineering*, *150*, 160–174. https://doi.org/10.1016/j.coastaleng.2019.04.004

Wiggins, M., Scott, T., Masselink, G., Mccarroll, R. J., & Russell, P. (2020). Predicting beach rotation using multiple atmospheric indices. *Marine Geology*, *426*(October 2019), 106207.

https://doi.org/10.1016/j.margeo.2020.106207

Winant, C. D., Inman, D. L., & Nordstrom, C. E. (1975). Description of seasonal beach changes using Empirical Eigenfunctions. *Journal of Geophysical Research*, *80*(15), 1979–1986.

Wright, L. D., Short, A. D., & Green, M. O. (1985). Short-term changes in the morphodynamic states of beaches and surf zones: An empirical predictive model. *Marine Geology*, *62*(3–4), 339–364. https://doi.org/10.1016/0025-3227(85)90123-9

Wu, Z., & Huang, N. E. (2004). A study of the characteristics of white noise using the empirical mode decomposition method. *Proceedings of the Royal Society A: Mathematical, Physical and Engineering Sciences*, *460*(2046), 1597–1611. https://doi.org/10.1098/rspa.2003.1221

Yates, M. L., Guza, R. T., & Reilly, W. C. O. (2009). Equilibrium shoreline response : Observations and modeling. *Journal of Geophysical Research*, *114*(September), 1–16. https://doi.org/10.1029/2009JC005359